Biological production in two contrasted regions of the Mediterranean Sea during the oligotrophic period: An estimate based on the diel cycle of optical properties measured by BGC-Argo profiling floats

Marie Barbieux[1], Julia Uitz[1], Alexandre Mignot[2], Collin Roesler[3], Hervé Claustre[1], Bernard Gentili[1], Vincent Taillandier[1], Fabrizio D'Ortenzio[1], Hubert Loisel[4], Antoine Poteau[1], Edouard Leymarie[1], Christophe Penkerc'h[1], Catherine Schmechtig[5], Annick Bricaud[1]

[1]CNRS and Sorbonne Université, Laboratoire d'Océanographie de Villefranche, LOV, 06230 Villefranche-sur-Mer, France

[2]Mercator Océan, 31520 Ramonville-Saint-Agne, France

[3]Bowdoin College, Earth and Oceanographic Science, Brunswick, Maine 04011, USA

[4]Université Littoral Côte d'Opale, Université Lille, CNRS, Laboratoire d'Océanologie et de Géosciences, 59000 Lille, France

[5]OSU Ecce Terra, UMS 3455, CNRS and Sorbonne Université, Paris 6, 4 place Jussieu, 75252 Paris CEDEX 05, France

Correspondence to: J. Uitz (julia.uitz@imev-mer.fr)

Abstract

This study assesses marine community production based on the diel variability of bio-optical properties monitored by two BioGeoChemical-Argo (BGC-Argo) floats. Experiments were conducted in two distinct Mediterranean systems, the Northwestern Ligurian Sea and the Central Ionian Sea, during summer months. We derived particulate organic carbon (POC) stock and gross community production integrated within the surface, euphotic and subsurface chlorophyll maximum (SCM) layers, using an existing approach applied to diel cycle measurements of the particulate beam attenuation (c_p) and backscattering (b_{bp}) coefficients. The diel cycle of c_p provided a robust proxy for quantifying biological production in both systems; that of b_{bp} was comparatively less robust. Derived primary production estimates vary by a factor of 2 depending upon the choice of the bio-optical relationship that converts the measured optical coefficient to POC, which is thus a critical step to constrain. Our results indicate a substantial contribution to the water column production of the SCM layer (16–42%), that varies largely with the considered system. In the Ligurian Sea, the SCM is a seasonal feature that behaves as a subsurface biomass maximum (SBM) with the ability to respond to episodic abiotic forcing by increasing production. In contrast, in the Ionian Sea, the SCM is permanent, primarily induced by phytoplankton photoacclimation and contributes moderately to water column production. These results clearly demonstrate the strong potential for transmissometers deployed on BGC-Argo profiling floats to quantify non-intrusively *in situ* biological production of organic carbon in the water column of stratified oligotrophic systems with recurring or permanent SCMs, which are widespread features in the global ocean.

1 Introduction

Primary production is an essential process in the global ocean carbon cycle (Field et al. 1998). As a major driver of the biological carbon pump, this biogeochemical process plays a critical role in the regulation of the Earth's climate (e.g. Sarmiento & Siegenthaler 1992; Falkowski 2012). Hence, quantifying primary production as a function of time and space in the ocean stands as a major challenge in the context of climate change. The balance between gross primary production and community respiration in the ocean determines the trophic status of marine systems, i.e. whether the system acts as a source or a sink of carbon (Williams 1993). This balance depends on the considered region and varies substantially according to spatial and temporal scales (Geider et al. 1997; Duarte & Agusti 1998; del Giorgio & Duarte 2002). It is therefore necessary to develop capabilities not only for assessing primary production on a global scale, but also for characterizing and quantifying the biogeochemical functioning of marine ecosystems at smaller spatial and temporal scales (Serret et al. 1999; González et al. 2001 and 2002).

Traditionally, primary production measurements are based on *in situ* or *in vitro* incubation experiments (i.e. on board the ship, under controlled conditions) coupled with isotopic carbon analysis (Nielsen 1952; Fitzwater et al. 1982; Dandonneau 1993; Barber & Hitling 2002) or measurements of oxygen concentration (Williams & Jenkinson 1982; Williams & Purdie 1991). These methods involve seawater sampling during field campaigns, sample manipulation and subsequent laboratory analyses, which are both time consuming and require strong technical expertise. As a result, the availability of field primary production measurements is relatively limited in terms of spatial and temporal coverage, which hinders the possibility of extrapolation to other systems or to larger space and time scales for modeling purposes. Active chlorophyll fluorescence techniques, such as Fast Repetition Rate Fluorometry (FRRF), yield in situ phytoplankton physiological parameters, which when combined with appropriate modeling,

provide estimates of derive primary production (e.g. Kolber & Falkowski 1993; Smyth et al. 2004). This technique has the major advantage of providing an instantaneous, fine-scale estimation of primary production in a non-invasive manner. Nevertheless, it is subject to assumptions and uncertainties, in particular related to the interpretation of fluorescence-light curve information in terms of carbon fixation, that still limit its use (see., e.g., Suggett et al. 2004; Corno et al. 2005; Regaudie-de-Gioux et al. 2014 and references herein).

Bio-optical primary production models coupled with ocean color satellite imagery represent another approach for obtaining primary production estimates (Morel 1991; Longhurst et al. 1995; Antoine et al. 1996; Behrenfeld et al. 2002). Such models are extremely valuable for assessing primary production with a large spatial coverage and over a broad range of temporal scales (Sathyendranath et al. 1995; Uitz et al. 2010; Chavez et al. 2011). Yet, most of these models suffer from several sources of uncertainty that can generate potential errors in the production estimates (e.g. Sarmiento et al. 2004; Saba et al. 2010; Saba et al. 2011). Sources of uncertainty include, in particular, the extrapolation of the satellite chlorophyll product, which is weighted to the upper portion of the euphotic zone, to the entirety of the productive region of the water column not sensed remotely. In addition, the *in situ*-based parameterization of phytoplankton photophysiology tends to lack robustness when applied to large (regional or global) scales and over seasonal to interannual time scales.

Diel cycles observed in bio-optical properties provide a less-empirical and more mechanistic approach to assess biological production. In a seminal paper published in 1989, Siegel et al. observed the *in situ* diurnal variability of the particulate beam attenuation coefficient (c_p) and used it as a surrogate for the diurnal variations in the abundance of biogenic particles and associated production in the oligotrophic North Pacific Ocean. Several studies subsequently pursued the investigation of the diurnal variability of marine bio-optical properties as a means for determining non-intrusively *in situ* biological production (e.g. Stramska &

89 Dickey 1992; Durand and Olson 1996; Claustre et al. 1999; Claustre 2008; Gernez et al. 2011;
90 White et al. 2017; Briggs et al. 2018).

91 Among this large body of literature, Claustre et al. (2008) carried further the principle of
92 the Siegel et al. (1989) approach for application to the South Pacific Subtropical Ocean. Based
93 upon the generally observed relationship between the c_p coefficient and the stock of particulate
94 organic carbon, POC (e.g. Stramski et al. 1999; Garner et al. 2006), Claustre et al. (2008)
95 assumed that diel variations in c_p reflect diel variations in POC. Thus, the observed daytime
96 increase and nighttime decrease in c_p-derived POC are used to estimate gross community
97 production, community losses and, assuming equivalent day and night losses, net community
98 production. Because the c_p coefficient is not specific to phytoplankton but includes the POC
99 contribution of both autotrophic and heterotrophic particles, the c_p-based method yields
100 estimate of community production.

101 Two studies (Kheireddine & Antoine 2014; Barnes & Antoine 2014) extended the
102 approach to the particulate backscattering coefficient (b_{bp}). The application opens up
103 opportunities for assessing community production from geostationary ocean color satellite
104 observations, from which a nearly continuous daytime b_{bp} coefficient can be retrieved. Both
105 studies focused on surface data obtained from moored observations from the Ligurian Sea
106 (Northwestern Mediterranean) and found that the diel cycle of b_{bp} may not necessarily be
107 interchanged with that of c_p, which calls for further investigations.

108 The optics-based approach has proven to be particularly relevant for appraising
109 particulate biological production in stratified oligotrophic systems such as subtropical gyres
110 (e.g. Siegel et al. 1998; Claustre et al. 2008; White et al. 2017). Interestingly, in such systems,
111 the biological production of organic carbon is difficult to quantify and potentially
112 underestimated by ^{14}C incubation methods (Juranek & Quay 2005; Quay et al. 2010). This
113 might be attributed to an inadequacy of traditional measurement methods for adequately

114 capturing the spatial and temporal heterogeneity of biological production that may exhibit local
115 or episodic events (Karl et al. 2003; Williams et al. 2004; McGillicuddy 2016). Moreover, in
116 stratified oligotrophic systems, the vertical distribution of phytoplankton is frequently
117 characterized by the presence of a deep chlorophyll maximum (DCM), also referred as
118 subsurface chlorophyll maximum (SCM; e.g. Cullen 1982; Hense & Beckmann 2008; Cullen
119 2015; Mignot et al., 2014). SCMs are not necessarily resolved by *in situ* discrete sampling and
120 cannot be observed from ocean color satellites that are limited to the surface ocean. They are
121 typically attributed to phytoplankton photoacclimation, the physiological process by which
122 phytoplankton cells adjust to light limitation by increasing their intracellular chlorophyll
123 content without concomitant increase in carbon (Kiefer et al. 1976; Cullen 1982; Fennel & Boss
124 2003; Letelier et al., 2004; Dubinsky & Stambler 2009). Yet, SCMs resulting from an actual
125 increase in phytoplankton (carbon) biomass, and so referred to as subsurface biomass maximum
126 (SBM), have also been observed episodically and/or seasonally in oligotrophic regions of the
127 global ocean (Beckmann & Hense 2007; Mignot et al. 2014; Barbieux et al. 2019; Cornec et al.
128 2021). Considering the large (45%) surface areas covered by stratified oligotrophic regions in
129 the global ocean (McClain et al. 2004), improving the quantification of biological production
130 of organic carbon and characterizing the contribution of SCMs to the water-column production
131 in such regions are critical. For this purpose, *in situ* diel-resolved measurements with high
132 spatio-temporal resolution in the entire water column represent an intriguing opportunity of
133 vital importance.

134 In this study, we exploit summertime observations acquired by two BioGeoChemical-
135 Argo (BGC-Argo) profiling floats deployed in contrasted systems of the Mediterranean Sea.
136 This offers a unique opportunity for pursuing the exploration of the bio-optical diel cycle-based
137 approach to biological production in oligotrophic environments. One of the two BGC-Argo
138 floats was deployed in the Ligurian Sea in the vicinity of the BOUSSOLE fixed mooring

(BOUée pour l'acquiSition d'une Série Optique à Long termE; Antoine et al. 2008). This area is representative of a seasonally stratified oligotrophic system, with a potentially productive SCM (e.g. Mignot et al. 2014; Barbieux et al. 2019) that follows a recurrent spring bloom. The second float was deployed in the Ionian Sea (Central Mediterranean) as part of the PEACETIME (ProcEss studies at the Air-sEa Interface after dust deposition in the MEditerranean sea) project (Guieu et al. 2020). The Ionian Sea is a nearly permanent oligotrophic system (e.g. Lavigne et al. 2015) with a SCM induced mostly by photoacclimation of phytoplankton cells without concomitant increase of carbon biomass (e.g. Mignot et al. 2014; Barbieux et al. 2019).

The BGC-Argo profiling floats used in this study measured, among a suite of physical and biogeochemical properties, the c_p and b_{bp} coefficients and were both programmed to sample the entire water column at a high temporal resolution (4 vertical profiles per 24h), in order to monitor the diel variations of the bio-optical properties. We applied, for the first time, a modified version of the method of Claustre et al. (2008) to the diel c_p and b_{bp} measurements acquired by the BGC-Argo floats to derive community production. Using this dataset, we (1) assess the relevance of the diel cycle-based method for estimating biological production of organic carbon in the considered regions and discuss the applicability of the method to b_{bp}, in addition to c_p; (2) investigate the regional and vertical variability of the production estimates with a focus on the SCM layer in relation to the biological and abiotic context; (3) discuss the relative contribution of the SCM layer to the water-column community production.

2 Data and methods

2.1 Study region

The Mediterranean Sea provides a unique environment for investigating the biogeochemical functioning of oligotrophic systems that exhibit either a seasonal or permanent

SCM. The Mediterranean is a deep ocean basin characterized by a West-to-East gradient in nutrients and chlorophyll *a* concentration (e.g. Dugdale & Wilkerson 1988; Bethoux et al. 1992; Antoine et al. 1995; Bosc et al. 2004; D'Ortenzio & D'Alcalà 2009) associated with a deepening of the SCM (Lavigne et al. 2012; Barbieux et al. 2019). The Ionian Sea in the eastern Mediterranean is defined as permanently oligotrophic, with the SCM settled at depth over the whole year. This system represents the oligotrophic end-member type of SCM (Barbieux et al. 2019), much like the subtropical South Pacific Ocean Gyre. By contrast, the Ligurian Sea in the western Mediterranean is seasonally productive akin to a temperate system (e.g. Casotti et al. 2003; Marty & Chiavérini 2010; Siokou-Frangou et al. 2010; Lavigne et al. 2015). The mixed layer deepens significantly during the winter period, inducing seasonal renewal of nutrients in the surface layer that supports the spring bloom (Marty et al. 2002; Lavigne et al. 2013; Pasqueron de Fommervault et al. 2015; Mayot et al. 2016). After the seasonal bloom, the SBM intensifies throughout the summer and into early fall. This system represents the temperate end-member type of SCM.

2.2 BGC-Argo multi-profiling floats and data processing

We deployed BGC-Argo floats programmed for "multi-profile" sampling in each of these two regions (Fig. 1). The Ligurian Sea float (hereafter noted fLig, WMO: 6901776), was deployed in the vicinity of the BOUSSOLE fixed mooring (7°54'E, 43°22'N) during one of the monthly cruises of the BOUSSOLE program (Antoine et al. 2008) and profiled from April 9, 2014 to March 15, 2015. For the purpose of this study focusing on oligotrophic systems, we selected the fLig float measurements acquired during the time period May 24 to September 13, 2014 to coincide in months with the Ionian Sea float time series. The Ionian Sea float (hereafter noted fIon, WMO: 6902828) was deployed as part of the PEACETIME project (Guieu et al. 2020). We used the fIon float measurements acquired during the time period May 28 to

September 11, 2017. Thus, although collected in different years, the data sets arise from similar seasonal contexts.

The BGC-Argo floats used in this study are "PROVOR CTS-4" (nke Instrumentation, Inc.). They were both equipped with the following sensors and derived data products: (1) a CTD sensor for depth, temperature and salinity; (2) a "remA" combo sensor that couples a Satlantic OCR-504 (for downwelling irradiance at three wavelengths in addition to photosynthetic available radiation, PAR) and a WET Labs ECO Puck Triplet (for both chlorophyll *a* (excitation/emission wavelengths of 470 nm/695 nm) and colored dissolved organic matter (CDOM; 370 nm/460 nm) fluorescence, and particulate backscattering coefficient at 700 nm); and (3) a WET Labs C-Rover (for particulate beam attenuation coefficient at 660 nm, 25-cm pathlength). Data were collected along water column profiles from 1000 m up to the surface with a vertical resolution of 10 m between 1000 and 250 m, 1 m between 250 and 10 m, and 0.2 m between 10 m and the surface. First, the BGC-Argo raw counts were converted into geophysical units by applying factory calibration. Second, we applied corrections following the BGC-Argo QC procedures (Schmechtig et al. 2015, 2016; Organelli et al. 2017).

Factory-calibrated chlorophyll fluorescence requires additional corrections for determining the chlorophyll *a* concentration (*Chl*). Values collected during daylight hours were corrected for non-photochemical quenching following Xing et al. (2012). A global analysis of factory-calibrated chlorophyll fluorescence measured with WET Labs ECO sensors relative to concurrent chlorophyll *a* concentrations, determined by High Performance Liquid Chromatography (HPLC), yielded a global overestimate bias of 2 (Roesler et al. 2017), with statistically significant regional biases varying between 0.5 and 6. The Mediterranean Sea is known to show very small regional variations of the fluorescence-to-*Chl* ratio (Taillandier et al. 2018), with a mean value close to 2 (1.66±0.28 and 1.72±0.23 for the Western and Eastern

Mediterranean, respectively; Roesler et al. 2017). Hence the bias correction factor of 2 was applied to BGC-Argo fluorescence data from both the Ligurian and Ionian regions, consistently with the processing performed at the Coriolis Data Center.

For the particulate backscattering coefficient (b_{bp}), we followed the BGC-Argo calibration and quality control procedure of Schmechtig et al. (2016). The backscattering coefficient at 700 nm (m^{-1}) is retrieved following Eq. (1):

$$b_{bp}(700) = 2\,\pi\,\chi\,[(\beta b_{bp} - Dark b_{bp}) \times Scale b_{bp} - \beta sw] \quad (1)$$

where $\chi = 1.076$ is the empirical weighting function that converts particulate volume scattering function at 124° to total backscattering coefficient (Sullivan et al. 2013); βb_{bp} is the raw observations from the backscattering meter (digital counts); $Dark b_{bp}$ (digital counts) and $Scale b_{bp}$ (m^{-1} sr^{-1} $count^{-1}$) are the calibration coefficients provided by the manufacturer; and βsw is the contribution to the Volume Scattering Function (VSF) by the pure seawater at the 700 nm measurement wavelength that is a function of temperature and salinity (Zhang et al. 2009).

The calibration procedure applied to the particulate beam attenuation coefficient (c_p) is similar to that described in Mignot et al. (2014). The beam transmission, T (%), is transformed into the beam attenuation coefficient, c (m^{-1}), using the relationship:

$$c = -\frac{1}{x} \ln \frac{T}{100} \quad (2)$$

where x is the transmissometer pathlength (25 cm). The beam attenuation coefficient c is the sum of the absorption and scattering by seawater and its particulate and dissolved constituents. At 660 nm, the contribution of CDOM (c_{CDOM}) can be considered negligible in oligotrophic waters because, although its absorption in the blue is comparable to that of particulate material (Organelli et al. 2014), the c_{CDOM} spectrum decays exponentially towards near zero in the red

(Bricaud et al. 1981), and because it is comprised of dissolved molecules and colloids, its scattering is negligible (Boss and Zaneveld 2003). Meanwhile $c_w(660)$ for pure water is constant and removed in the application of the factory calibration; effects due to dissolved salt are accounted for according to Zhang et al. (2009). Hence, at a wavelength of 660 nm, the particle beam attenuation coefficient, c_p (m^{-1}), is retrieved by subtracting the seawater contribution to c. The biofouling-induced signal increase that is observed in clear deep waters and results in a drift in c_p values with time, is corrected as follows. For each profile, a median c_p value, used as an "offset", is computed from the c_p values acquired between 300 m and the maximum sampled depth, and subtracted from the entire profile.

Using the solar noon Photosynthetically Available Radiation (PAR) measurements, we computed the euphotic layer depth (Z_{eu}) as the depth at which the PAR is reduced to 1% of its value just below the surface (Gordon & McCluney 1975) and the penetration depth (Z_{pd}; also known as the e-folding depth or first attenuation depth) as Z_{eu} / 4.6. We define the surface layer from 0 m to Z_{pd}. We also define the SCM layer as in Barbieux et al. (2019), whereby a Gaussian model is fit to each *Chl* vertical profile measured by the floats in order to determine the depth interval of the full width half maximum of the SCM. Finally, the Mixed Layer Depth (MLD) is derived from the float CTD data as the depth at which the potential density difference relative to the surface reference value is 0.03 kg m^{-3} (de Boyer Montégut et al. 2004).

Unlike the majority of BGC-Argo floats that collect profile measurements every 10 days, the two platforms used in this study sampled the water column with 4 profiles per day, albeit with slightly different regimes (Fig. 2). The fLig float cycle commences with the first profile at sunrise (t_{sr}), a second at solar noon (t_n), a third profile at sunset the same day (t_{ss}), and a fourth profile at sunrise the next day (t_{sr+1}). The fLig float then acquires a profile at solar noon 4 days later (t_{n+4}), and then restarts 3 days later the acquisition of 4 profiles in 24 hours from sunrise (t_{sr+7}). The fIon cycle is performed over a single 24-hour period; it begins at sunrise (t_{sr}),

followed by a second profile at solar noon (t_n), a third at sunset (t_{ss}) and a last night profile at approximately midnight (t_m). For this float, the sampling cycle is repeated each day.

2.3 Characterization of the diel cycle of the bio-optical properties

In order to characterize the amplitude and variability of the diel cycle of the c_p and b_{bp} coefficients, we use the metrics defined by Gernez et al. (2011) and Kheireddine & Antoine (2014). First, we compute the amplitude of the diurnal variation of the c_p and b_{bp} coefficients as:

$$\Delta c_p = c_p(t_{ss}) - c_p(t_{sr}) \quad (3a)$$

$$\Delta b_{bp} = b_{bp}(t_{ss}) - b_{bp}(t_{sr}) \quad (3b)$$

with $c_p(t_{sr})$ and $b_{bp}(t_{sr})$ the values of c_p and b_{bp} at sunrise and $c_p(t_{ss})$ and $b_{bp}(t_{ss})$ the values at sunset the same day.

We also consider the relative daily variation $\tilde{\Delta}c_p$ and $\tilde{\Delta}b_{bp}$ (expressed as % change) for each float and each day of observation, from sunrise to sunrise as follows:

$$\tilde{\Delta}c_p = 100\,(\frac{c_p(t_{sr})}{c_p(t_{sr+1})} - 1) \quad (4a)$$

$$\tilde{\Delta}b_{bp} = 100\,(\frac{b_{bp}(t_{sr})}{b_{bp}(t_{sr+1})} - 1) \quad (4b)$$

with $c_p(t_{sr})$ and $b_{bp}(t_{sr})$ being the values of c_p and b_{bp} at sunrise and $c_p(t_{sr+1})$ and $b_{bp}(t_{sr+1})$ the values at sunrise the next day. Then the mean and range in relative daily variations ($\widetilde{m\Delta}$ and $\widetilde{r\Delta}$, respectively) are computed for each float over the entire time series.

2.4 Principle of the bio-optical diel cycle-based approach to biological production

The two bio-optical properties that we considered in this study, c_p and b_{bp}, are both linearly correlated to, and thus may be used as a proxy for, the stock of POC (e.g. Oubelkheir et al. 2005; Gardner et al. 2006; Cetinić et al. 2012). Both of these bio-optical proxies have been

shown to exhibit a diurnal cycle (e.g. Oubelkheir & Sciandra 2008; Loisel et al. 2011; Kheireddine & Antoine 2014). The daily solar cycle is a major driver of biological activity in all oceanic euphotic zones, which influences the abundance of microorganisms, including phytoplankton (Jacquet et al. 1998; Vaulot & Marie 1999; Brunet et al. 2007) and heterotrophic bacteria (Oubelkheir & Sciandra 2008; Claustre et al. 2008) and, therefore, the magnitude of the c_p and b_{bp} coefficients. Diel changes in the c_p or b_{bp} coefficient reflect processes that affect the cellular abundance (number) and the attenuation, or backscattering, cross-section, which varies with cell size and refractive index. The diurnal increase in c_p or b_{bp} has primarily been attributed to photosynthetic cellular organic carbon production (Siegel et al. 1998), that will first result in an increase in cell size, or an increase in cell abundance and a decrease in cell size following cell division often occurring at night. In addition, the diurnal increase in c_p or b_{bp} may be caused by variations in cellular shape and refractive index that accompany intracellular carbon accumulation (Stramski & Reynolds 1993; Durand & Olson 1996; Claustre et al. 2002; Durand et al. 2002). The nighttime decrease in c_p or b_{bp} may be explained by a decrease in cellular abundance due to aggregation, sinking or grazing (Cullen et al. 1992), a reduction in cell size and/or refractive index associated with cell division and respiration, the latter involving changes in intracellular carbon concentration with effect on the refractive index (Stramski & Reynolds 1993). Community composition and cell physiology (in response to diel fluctuations of the light field) might also influence the optical diel variability through their effects on cell size and refractive index. Diel variation in photoacclimation can be important in coastal communities dominated by microplankton (Litaker et al. 2002; Brunet et al. 2008). Nevertheless, previous studies conducted in oligotrophic environments suggest that photosynthetic growth is the major driver of the diurnal changes in c_p or b_{bp} (Gernez et al. 2002; Claustre et al. 2008). In addition, Claustre et al. (2002), in an experimental work based on *Prochlorococcus*, a frequent taxon in oligotrophic regions, show that although non-negligible,

307 the diel variability in photoacclimation is much less pronounced than that in phytoplankton
308 growth.

309 Following a modified version of Claustre et al. (2008), the observed daytime increase and
310 nighttime decrease in c_p-derived (or b_{bp}-derived) POC are used to estimate gross community
311 production. For this purpose, the c_p and b_{bp} coefficients, measured *in situ* by the BGC-Argo
312 profiling floats, are converted into POC equivalent using a constant c_p-to-POC (or b_{bp}-to-POC)
313 relationship from the literature (see below). By definition, the c_p and b_{bp} coefficients target
314 particles so that the dissolved biological matter is not accounted for by the present method.

315 **2.5 Bio-optical properties-to-POC relationships**

316 The conversion of c_p and b_{bp} into POC relies on the use of empirical proxy relationships
317 and assumptions concerning the variations in those relationships. First, as in Claustre et al.
318 (2008), we assume that the c_p- or b_{bp}-to-POC relationship remains constant on a daily timescale,
319 consistently with previous works (Stramski & Reynolds 1993; Cullen & Lewis 1995), so that
320 observed variations in the optical coefficients can be interpreted as variations in POC. Second,
321 the specific proxy value is not constant, as many empirical relationships between POC and c_p
322 (e.g. Claustre et al. 1999; Oubelkheir et al. 2005; Gardner et al. 2006; Loisel et al. 2011) or b_{bp}
323 (e.g. Stramski et al. 2008; Loisel et al. 2011; Cetinić et al. 2012) have been proposed for specific
324 regions (Tables 1 and 2). In the present study, we used the relationships from Oubelkheir et al.
325 (2005) and Loisel et al. (2011) for c_p and b_{bp}, respectively. Both relationships were established
326 from *in situ* measurements collected in the Mediterranean Sea and produce c_p- or b_{bp}-derived
327 POC values falling in the middle of the range of all the POC values resulting from the different
328 bio-optical relationships taken from the literature (Tables 1 and 2).

2.6 Estimating biological production from the diel cycle of POC

2.6.1 Hypotheses

The time-rate-of-change in depth-resolved POC biomass, $b(z,t)$, can be described by a partial differential equation:

$$\frac{\partial b(z,t)}{\partial t} = \mu(z,t)\, b(z,t) - l(z,t)\, b(z,t), \quad (5)$$

where $\mu(z,t)$ is the particle photosynthetic growth rate and $l(z,t)$ the particle loss rate at depth z and time t (both in units of d^{-1}). As in previous studies (Claustre et al. 2008, Gernez et al. 2011; Barnes and Antoine 2014), we assume a 1D framework. In other words, we ignore the effects of lateral transport of particles by oceanic currents and assume that there is no vertical transport of particles into or out of the layer considered. We also assume that the loss rate is constant throughout the day and uniform with depth, i.e. $l(z,t) = l$. In this context, the time series of profiles are first converted to depth-integrated biomass (from $b(z,t)$ to $B(t)$) for each of the layers in question, and then integrated over time to determine daytime gain, nighttime loss, and net daily production.

2.6.2 Calculation of the loss rate

During nighttime, there is no photosynthetic growth, so that Eq. (5) becomes:

$$\frac{\partial b(z,t)}{\partial t} = l\, b(z,t). \quad (6)$$

The integration of Eq. (6) over depth yields an expression of the rate of change of the depth-integrated POC biomass, $B(t)$:

$$\frac{\partial B(t)}{\partial t} = -\, l\, B(t), \quad (7)$$

with $B(t) = \int_{z2}^{z1} b(z,t)\mathrm{d}z$, the POC integrated within a given layer of the water column, comprised between the depths z_1 and z_2 (in gC m^{-2}). In this respect, we consider three different

layers: the euphotic layer extending from z_1 = 0 m to $z2 = Z_{eu}$; the surface layer extending from z_1 = 0 m to $z2 = Z_{pd}$; and the SCM layer extending from $z1 = Z_{SCM} - Z_{SCM,1/2}$ and $z2 = Z_{SCM} + Z_{SCM,1/2}$, with Z_{SCM} the depth of the SCM and $Z_{SCM,1/2}$ the depth at which *Chl* is half of the SCM value.

Eq. (7) can be integrated over nighttime to obtain an equation for the loss rate l, as a function of the nocturnal variation of B:

$$l = \frac{\ln\left(\frac{B_{ss}}{B_{sr+1}}\right)}{t_{sr+1} - t_{ss}}, \quad (8)$$

with $B(t_{ss})$ and $B(t_{sr+1})$ corresponding to the POC integrated within the layer of interest, at t_{ss} (sunset) and t_{sr+1} (sunrise of the next day).

2.6.3 Calculation of the production rate

The daily (24-hour) depth-integrated gross production of POC, P (in units of gC m^{-2} d^{-1}), is defined as:

$$P = \int_{t_{sr}}^{t_{sr+1}} \int_{z2}^{z1} \mu(z,t)\, b(z,t)\, \mathrm{d}z\, \mathrm{d}t, \quad (9)$$

with t_{sr} the time of sunrise on day 1 and t_{sr+1} the time of sunrise the following day. Equation (5) can be used to express P as a function of l, $b(z,t)$, and the rate of change of $b(z,t)$:

$$P = \int_{t_{sr}}^{t_{sr+1}} \int_{z2}^{z1} \left(\frac{\partial b(z,t)}{\partial t} + l\, b(z,t)\right) \mathrm{d}z\, \mathrm{d}t, \quad (10)$$

which yields:

$$P = B_{t_{sr+1}} - B_{t_{sr}} + l \int_{t_{sr}}^{t_{sr+1}} B(t)\, \mathrm{d}t. \quad (11)$$

where the gross production P is calculated as the sum of the net daily changes in POC biomass plus POC losses, assuming a constant rate (l) during daytime and nighttime.

Finally, using the trapezoidal rule, Eq. (11) simplifies into

$$P = B_{t_{sr+1}} - B_{t_{sr}} + l \sum_{i=1}^{j} (t_{i+1} - t_i) \frac{B_{i+1} + B_i}{2}, \quad (12)$$

with l calculated from Eq. (8) and the index i corresponding to the different measurement time steps over the course of the diel cycle (t_{sr}, t_n, t_{ss}, and t_{sr+1}; Fig. 2).

In summary, Eq. (12) is applied to the time series of the BGC-Argo floats by using b_{bp} and c_p converted into POC equivalents, integrated within the euphotic, surface, and SCM layers to compute c_p- and b_{bp}-derived estimates of gross community production, P, in all three layers of the water column.

2.7 Primary production model

The community production estimates obtained from the bio-optical diel cycle-based method are evaluated against primary production values computed with the bio-optical primary production model of Morel (1991). Morel's model estimates the daily depth-resolved organic carbon concentration fixed by photosynthesis, using the noontime measurements of *Chl*, temperature and PAR within the water column by the BGC-Argo profiling floats as model inputs. The standard phytoplankton photophysiological parameterization is used for these calculations (Morel 1991; Morel et al. 1996).

2.8 Phytoplankton pigments and community composition

During the BOUSSOLE cruises conducted in 2014 (cruises #143 to #154) and the PEACETIME cruise, discrete seawater samples were taken at 10–12 depths within the water column from Niskin bottles mounted on a CTD-rosette system and then filtered under low vacuum onto Whatman GF/F filters (0.7-µm nominal pore size, 25-mm diameter). The filters were flash-frozen in liquid nitrogen and stored at -80°C until analysis by HPLC following the protocol of Ras et al. (2008). The concentrations of phytoplankton pigments resulting from these analyses were used to estimate the composition of the phytoplankton assemblage. For this purpose, we used the diagnostic pigment-based approach (Claustre et al. 1994; Vidussi et al.

2001; Uitz et al. 2006) with the coefficients of Di Cicco et al. (2017) to account for the specificities of Mediterranean phytoplankton communities. This approach yields the relative contribution to chlorophyll *a* biomass of major taxonomic groups merged into three size classes (micro-, nano and picophytoplankton).

The fLig float was spatially distanced from the location of sampling at the BOUSSOLE mooring site. Thus, it was necessary to identify the time shift for matching the cruise-sampled analyses to the float profile measurements. This was achieved by performing a cross-correlation analysis of the bio-optical timeseries measurements collected on the float with that on the mooring (in this case *Chl*, c_p and b_{bp}). A positive time lag between the BOUSSOLE site and the position of the fLig float during its drift is observed suggesting that the variations observed by the float led that observed at BOUSSOLE by ~2 days. This small-time lag coupled with high correlation coefficient values and long decorrelation time scales, indicate that the monthly interpolated pigment data measured at the BOUSSOLE site may be considered as representative of the pigment composition along the fLig float trajectory.

3 Results and discussion

We first provide an overview of the biogeochemical and bio-optical characteristics measured by the two BGC-Argo profiling floats in the Ligurian and Ionian Seas. We then assess the usefulness of the diel cycle of the b_{bp} coefficient for deriving community production, in comparison to the c_p-derived estimates as a reference, and discuss the c_p-derived estimates. Finally, we examine the community production estimates in both study regions, with an emphasis on the SCM layer and its biogeochemical significance.

3.1 Biogeochemical and bio-optical context in the study regions

Both study regions are characterized by either seasonal or persistent oligotrophy, with mean surface *Chl* values ranging within 0.08–0.22 mg m^{-3} (Fig. 3), and a stratified water column with a consistently shallow MLD (<30 m). They do exhibit very different euphotic depths, with a mean Z_{eu} of 47±5 m and 89±4 m in the Ligurian and Ionian Seas, respectively. Consistently, the instantaneous midday PAR values are much lower in the upper layer of the Ligurian Sea (93±70 µE m^{-2} s^{-1}) than in the Ionian Sea (500±60 µE m^{-2} s^{-1}) and shows a more rapid decrease within the water column as phytoplankton biomass absorbs light. Both regions also display a SCM, the depth of which co-occurs with Z_{eu} and the isopycnal 28.85 (i.e. the isoline of potential density 28.85 kg m^{-3}) over the considered time series, except for the last month of observation in the Ionian Sea.

In the Ligurian Sea, the SCM is intense (1.06±0.34 mg Chl m^{-3}; Fig. 3a), relatively shallow (41±7 m), and associated with the subsurface c_p and b_{bp} maxima (0.27±0.09 and 0.0015±0.0006 m^{-1}, respectively; Fig. 3b–c). The *Chl* and c_p values are 5 times larger in the SCM layer than at surface, and the b_{bp} values 3.6 times larger. In contrast, in the Ionian Sea, the SCM is associated with lower values of *Chl* (0.27±0.07 mg m^{-3}; Fig. 3d), c_p (0.05±0.01 m^{-1}; Fig. 3e) and b_{bp} (0.0005±0.0001 m^{-1}; Fig. 3f). Compared to the Ligurian Sea SCM, the Ionian Sea SCM is located twice as deep (97±11 m) and is uncoupled from the c_p and b_{bp} maxima that occur at shallower depth.

Hence, the selected regions are representative of two contrasted SCM systems with distinct degree of oligotrophy, consistent with our expectations (e.g. D'Ortenzio & Ribera D'Alcalà 2009; Barbieux et al. 2019). Such a contrast in the SCM characteristics in relation with the trophic gradient of the environment has already been observed in the Mediterranean Sea (e.g. Lavigne et al. 2015; Barbieux et al. 2019) and on a global scale (e.g. Cullen 2015 and references therein; Mignot et al. 2014; Cornec et al. 2021). These studies report that the depth

of the SCM is inversely correlated with the surface *Chl* (an index of the trophic status) and light attenuation within the water column. Previous studies (Mignot et al. 2014; Barbieux et al. 2019; Cornec et al. 2021) indicate that moderately oligotrophic, temperate conditions are generally associated with a relatively shallow SCM coupled to a maximum in c_p or b_{bp}, reflecting an increase in phytoplankton carbon biomass (SBM). In contrast, in the most oligotrophic environments, the vertical distribution of *Chl* shows a maximum at greater depths and is decoupled from the c_p or b_{bp} vertical distribution. Furthermore, Barbieux et al. (2019) show that, in the northwestern Mediterranean region, the SCM mirrors a biomass maximum located slightly above Z_{eu}, which benefits from an adequate light-nutrient regime thanks to a deep winter convective mixing allowing nutrient replenishment in the upper ocean. In the Ionian Sea where the MLD and nutricline are permanently decoupled, the SCM establishes below Z_{eu} as phytoplankton organisms attempt to reach nutrient resources. Prevailing low-light conditions lead to pronounced photoadaptation of phytoplankton. Thus, consistently with previous work, the present observations indicate that the Ligurian Sea SCM is a phytoplankton carbon biomass (SBM) likely resulting from favorable light and nutrient conditions, whereas the Ionian SCM would be essentially induced by photoacclimation of phytoplankton cells.

Although the summer period is typically considered stable, some temporal variations are observed over the time series that are more pronounced in the SCM layer than at surface. In the Ligurian Sea SCM, the *Chl*, c_p and b_{bp} exhibit similar temporal evolution, with relatively high values in late May 2014, followed by a marked decrease until mid-July (Figs. 4a–c). Then we observe two local minima in *Chl*, c_p and b_{bp} that delineate a second peak between July 14 and August 16, 2014 (as indicated by the dashed lines in Fig. 4a–c). In the Ionian Sea SCM, the *Chl*, c_p and b_{bp} values all decrease from late May until a minimum is reached on August 11, 2017 (dashed line in Figs. 4d–e) and a second increase is recorded later in the season. These

466 temporal patterns are further discussed in relation with the variability in the estimated POC and
467 production rates (Section 3.4).

468 **3.2 Assessment of the method**

469 **3.2.1 Analysis of the diel cycle of the c_p and b_{bp} coefficients**

470 Diel cycles, characterized by a daytime increase and a nighttime decrease, are observed in
471 both c_p and b_{bp} time series in all layers of the water column, as illustrated for the SCM layer of
472 the Ionian Sea in Fig. 5 (examples of the diel cycles of c_p and b_{bp} for both the Ligurian and
473 Ionian Seas are provided in Appendix A). Considering the time series of the Ligurian and Ionian
474 Seas, as well as the surface and SCM layers, the c_p and b_{bp} coefficients show mean diurnal
475 amplitudes, Δc_p and Δb_{bp}, spanning between 0.001 m^{-1} and 0.02 m^{-1} and 7 x 10^{-6} m^{-1} and 9 x
476 10^{-5} m^{-1}, respectively. These results are consistent with Gernez et al. (2011), who observed Δc_p
477 values ranging within 0.01 m^{-1} and 0.07 m^{-1} in the surface layer of the Ligurian Sea
478 (BOUSSOLE mooring) during the summer to fall oligotrophic period. Relative to the mean c_p
479 and b_{bp} values, the mean Δc_p and Δb_{bp} correspond to diurnal variations of 9–20% and 5–10%,
480 respectively.

481 In the surface layer of the Ligurian Sea, the diel cycles of c_p and b_{bp} exhibit, respectively,
482 mean relative daily variation ($\widetilde{m\Delta}$) of 12.7% and 2.3%, and a range in relative daily variations
483 ($\widetilde{r\Delta}$) of 256.7% and 28.5% (Table 3). These values are of the same order of magnitude as those
484 reported by Kheireddine & Antoine (2014), acquired from the BOUSSOLE surface mooring in
485 the same area and during the oligotrophic season (from -5% to 25% for c_p and from -2% to 10%
486 for b_{bp}). Interestingly, the diel cycle of the c_p coefficient appears systematically more
487 pronounced than that of b_{bp}, with larger values of $\widetilde{m\Delta}$ and $\widetilde{r\Delta}$, regardless of the considered
488 region and layer of the water column (Table 3).

To first order, the variability in the b_{bp} and c_p coefficients is determined by the variability in particle concentration, which underpins their robustness as POC proxies in open-ocean conditions and explains their coherent evolution on a monthly timescale (Figs. 3–4). Nevertheless, to second order, these coefficients vary differentially with the size and composition of the particle pool. In particular, phytoplankton make a larger contribution to c_p than b_{bp}, in part due to their strong absorption efficiency. In addition, b_{bp} is more sensitive to smaller (<1 μm) particles (Stramski & Kiefer 1991; Ahn et al. 1992; Stramski et al. 2001; Boss et al. 2004) and to particle shape and internal structure (Bernard et al. 2009; Neukermans et al. 2012; Moutier et al. 2017; Organelli et al. 2018). While the diel cycle of c_p would be essentially driven by photosynthetic processes due to the influence of phytoplankton on c_p, b_{bp} would be more responsive to detritus and/or heterotrophic bacteria that show minor, if not negligible, daily variability. Hence, such specificities in the bio-optical coefficients may explain the observed differences in their diel cycles.

Based on high-frequency surface measurements in the Ligurian Sea in various seasons, the studies of Kheireddine & Antoine (2014) and Barnes & Antoine (2014) demonstrated that the diel cycle of b_{bp} not only exhibits much reduced relative amplitude compared to that of c_p, but the features of the b_{bp} cycle are not synchronous with that of the c_p cycle. Thus, b_{bp} cannot be used interchangeably with c_p for assessing daily changes in POC or community production, but perhaps provides additional information on the particulate matter and its production rates. Our results support these previous findings, not only for the surface layer of the Ligurian Sea, but also for the whole water column of both the Ligurian and Ionian regions.

We now consider the integrated euphotic zone gross community production estimates derived from the bio-optical diel cycle-based method (Fig. 6). We compare the c_p- and b_{bp}-based estimates with primary production estimates computed with the model of Morel (1991). The b_{bp}-derived production rates underestimate those derived from c_p in both regions by about

514 a factor of ten, with respective mean values of 0.11±0.28 gC m^{-2} d^{-1} and 1.18 ±1.13 gC m^{-2} d^{-1}
515 in the Ligurian Sea, and 0.04±0.04 gC m^{-2} d^{-1} and 0.46 ±0.11 gC m^{-2} d^{-1} in the Ionian Sea. In
516 addition, the b_{bp}-derived production is much lower than the primary production computed with
517 the model of Morel (1991), which has mean values of 0.91±0.14 gC m^{-2} d^{-1} in the Ligurian Sea
518 and 0.31 ±0.04 gC m^{-2} d^{-1} in the Ionian Sea. The significantly lower community production
519 rates are a direct effect of the dampened relative daily amplitude of the b_{bp} diel cycle (Table 3),
520 and the sensitivity of b_{bp} to the smaller heterotrophic and detrital particulate matter. The bio-
521 optical diel cycle-based method, whether applied to c_p or b_{bp}, yields an estimate of the
522 community production, i.e. that associated with the accumulation of phytoplankton *and* bacteria
523 biomass, which is necessarily larger than the primary (photo-autotrophic) production rates from
524 the Morel (1991) model. These questionable low values of community production, along with
525 the observation of a weak daily variability in b_{bp}, support the idea that the diel cycle of b_{bp} may
526 not be a reliable index for total community production rates, consistently with previous studies
527 (Kheireddine & Antoine 2014; Barnes & Antoine 2014). However, the utility of a b_{bp}-derived
528 community production may be revealed in elucidating rates for distinct size-based groups of
529 organisms, such as picoplankton. A better understanding of the specific size range that
530 dominates the diel cycle in b_{bp} will be important to understand. Yet, for our purposes, we
531 disregard the b_{bp}-based estimates and focus our analysis on the c_p-derived gross community
532 production estimates.

533 **3.2.2 Community production derived from the c_p coefficient**

534 The c_p-derived estimates of gross community production, integrated within the euphotic
535 layer, compare favorably with those found in the literature for similar Mediterranean areas (see
536 Table 4 and references therein). The c_p-based estimates show a 2.5-fold difference between the
537 Ligurian Sea and the Ionian Sea (mean of 1.18 gC m^{-2} d^{-1} and 0.46 gC m^{-2} d^{-1}, respectively;
538 Table 6). In comparison, water column-integrated primary production values, either inferred

539 from satellite observations and biogeochemical models or measured *in situ*, vary within the
540 range 0.13–1 gC m^{-2} d^{-1} and 0.14–0.69 gC m^{-2} d^{-1} for the Western (or Ligurian) and Eastern (or
541 Ionian) region, respectively (Table 4). As expected, our c_p-based community production rates
542 are larger than published primary production rates. The present c_p-derived values also compare
543 favorably with gross community production estimates inferred from a similar approach applied
544 to bio-optical measurements from the BOUSSOLE mooring in the Ligurian Sea (0.5–0.8 gC m^{-2}
545 d^{-1} in Gernez et al. 2011; 0.8–1.5 gC m^{-2} d^{-1} in Barnes & Antoine 2014) and along an
546 oligotrophic gradient in the South Pacific Subtropical Ocean (0.85 gC m^{-2} d^{-1}; Claustre et al.
547 2008).

548 The empirical relationships linking the c_p (or b_{bp}) coefficient to POC are known to exhibit
549 regional and seasonal variability in response to changes in the composition of the particle
550 assemblage and associated changes in particle size, shape and type, i.e. biogenic or mineral
551 (e.g. Stramski et al. 2004; Neukermans et al. 2012; Slade & Boss 2015). Hence, the choice of
552 such relationships strongly affects the conversion of the measured daily bio-optical variability
553 into POC fluxes. For the time period and study regions here, the c_p-based community
554 production varies by a factor of 2, depending on the selected bio-optical relationship, so that c_p-
555 based estimates vary between 0.89±0.84 gC m^{-2} d^{-1} and 1.62±1.54 gC m^{-2} d^{-1} in the Ligurian
556 Sea, and between 0.35±0.09 gC m^{-2} d^{-1} and 0.63±0.16 gC m^{-2} d^{-1} in the Ionian Sea. The minimal
557 and maximal values are obtained with the bio-optical relationships from Marra et al. (1995) and
558 Stramski et al. (2008), respectively (Table 5). Compared to the reference value obtained using
559 the Oubelkheir et al. (2005) relationship, the c_p-based estimates are 25% lower and 37% higher
560 using the relationships of Marra et al. (1995) and Stramski et al. (2008), respectively. We also
561 note that using the Mediterranean relationship of Loisel et al. (2011), instead of that of
562 Oubelkheir et al. (2005), would reduce the c_p-based estimates by 17% in both study regions

563 (Table 5). That said, although the absolute magnitudes vary depending upon proxy choice, the
564 differences observed between locations is robust.

565 The use of the single relationship established from Mediterranean waters (Oubelkheir et al.
566 2005) appears as a reasonable choice for the study region. Yet, if more relevant bio-optical
567 proxy relationships are available, such as one that accounts for spatial and seasonal variations,
568 and even applicable to different layers of the water column, that would certainly reduce the
569 uncertainty in the rate estimation. Although this is beyond the scope of the present study, we
570 recognize that such investigations should be conducted in the future in order to refine optics-
571 based biomass (POC) and community production estimates.

572 **3.3 Regional and vertical variability of production**

573 The temporal evolution of the c_p-derived POC biomass integrated within the three distinct
574 layers of the water column is presented for the two study regions in Fig. 7. The integrated POC
575 concentration values follow similar temporal trends as reported for c_p (Figs. 3–4). In the
576 Ligurian Sea, the euphotic layer-integrated POC varies between 1.5 and 6.0 gC m^{-2} (mean of
577 3.7±1.1 gC m^{-2}; Fig. 7a and Table 6). There was a decrease from late May to mid-July (6.0 to
578 1.5 gC m^{-2}) followed by a moderate peak (3.9 gC m^{-2}) between mid-July and mid-August (as
579 bounded by the dashed lines in Fig. 5). The c_p-based community production did exhibit large
580 variability over the time period (Fig. 7b and Table 6), but interestingly, the moderate POC peak
581 observed in the core of the oligotrophic season (between mid-July and mid-August) is
582 associated with the maximum production rate of the time series (4.3 gC m^{-2} d^{-1}).

583 In the Ionian Sea, the POC biomass integrated within the euphotic zone is much lower
584 than in the Ligurian Sea and remains more stable over the time period (1.9±0.24 gC m^{-2}; Fig.
585 7c and Table 6). As with POC, the community production is much lower in the Ionian Sea than
586 in the Ligurian Sea, but still exhibits substantial variability with values ranging within 0.06–

587 0.68 gC m^{-2} d^{-1} (Fig. 7d). These results are consistent with multiple studies reporting a large
588 difference in the trophic status and productivity of the Ligurian and Ionian Seas, on seasonal
589 and annual timescales (D'Ortenzio & Ribera d'Alcala, 2009; Siokou-Frangou et al. 2010;
590 Lavigne et al. 2013; Mayot et al. 2016). Our results confirm this difference, yet on a monthly
591 timescale during the oligotrophic summer period.

592 The gross community production estimates integrated over different layers of the water
593 column reveal distinct patterns. In the Ligurian Sea, both the euphotic and SCM layers show
594 large production rates (0.96±1.3 gC m^{-2} d^{-1}), with production in the SCM layer frequently
595 equaling or overtaking on the production in the euphotic layer (Fig. 7b). This is particularly
596 striking in late July, when the production peak is actually associated with a large enhancement
597 of the production in the SCM layer (4.9 gC m^{-2} d^{-1}). In contrast, the surface layer shows reduced
598 production rates (0.29±0.33 gC m^{-2} d^{-1}), a pattern also observed in the Ionian Sea (0.11±0.04
599 gC m^{-2} d^{-1}). In the Ionian Sea, the production is maximal in the euphotic zone, and very variable
600 and occasionally larger in the SCM layer (0.14±0.39 gC m^{-2} d^{-1}; Fig. 7d). The bio-optical diel
601 cycle-based method produces several occurrences of negative values in the SCM layer,
602 indicating that the 1D assumption is occasionally not satisfied in the lower part of the euphotic
603 layer. This could arise when physical processes that transport particles are larger than local
604 growth and loss of POC.

605 Our results support the hypothesis raised in previous studies (e.g. Mignot et al. 2014;
606 Barbieux et al. 2019) that, in the Ligurian temperate-like system, the SCM, which is in fact a
607 SBM, may be highly productive. Conversely, in the Ionian region, which shows similarities
608 with subtropical stratified oligotrophic systems, the SCM primarily reflects photoacclimation
609 and is less productive. Beyond these mean regional trends, both SCM systems exhibit some
610 temporal variability in production, a somewhat unexpected pattern at the core of the presumably
611 stable oligotrophic season.

3.4 Production in the SCM layer in relation with the biotic and abiotic context

Here we investigate the temporal variability in the SCM layer production and attempt to interpret the observed patterns in the context of biological and abiotic conditions.

3.4.1 Phytoplankton and particulate assemblage

The pigment data collected during the BOUSSOLE and PEACETIME cruises concomitantly with the deployments of the fLig and fIon floats, respectively, are used as proxies for phytoplankton community structure (Fig. 8). In the Ligurian Sea, nanophytoplankton (mainly prymnesiophytes) appear as dominant contributors to the phytoplankton assemblage both in the surface layer (48±8%; Fig. 8b) and SCM layer (54±10%). Picophytoplankton (prokaryotes and small chlorophytes) and microphytoplankton (diatoms and dinoflagellates) are present in moderate proportions, with 30±11% and 22±5% in the upper layer, and 19±7% and 27±9% in the SCM layer, respectively (Figs. 8a and 8c). No marked shift in the community composition is observed during the timeseries, although occasional increase in the contribution of microphytoplankton is observed in the SCM layer, with no clear temporal trend (Fig. 8a and Appendix B). In the Ionian Sea, the surface layer displays large contribution of nanophytoplankton (56±2%; Fig. 8e) and, to a lesser extent, picophytoplankton (29±3%; Fig. 8d). However, the SCM level is characterized by an enhanced contribution of microphytoplankton (diatoms) to the algal assemblage (49±5%; Fig. 8f), as discussed in Marañón et al. (2021). The Ionian PEACETIME data was limited to the period from May 25 to 28, 2017, and thus it was not possible to determine whether the composition of phytoplankton communities evolved with time. Although not characterized by the prokaryotic populations (*Synechococcus* and *Prochlorococcus*) that typically prevail in stratified oligotrophic environments, our observations are consistent with previous studies reporting enhanced contributions of nanophytoplankton (e.g. Gitelson et al. 1996; Vidussi et al. 2001) and the

636 occurrence of diatoms at depth (Siokou-Frangou et al. 2010; Crombet et al. 2011; Marañón et
637 al. 2021) in the Mediterranean Sea.

638 Bio-optical properties and their ratios provide indication about variations in the constituents
639 (algal or nonalgal) and size of the particulate pool, the composition of the phytoplankton
640 assemblage and the physiological status of phytoplankton cells (e.g. Geider 1987; Ulloa et al.
641 1994; Stramski et al. 2004; Loisel et al. 2007). Here we consider the bio-optical ratios b_{bp} / c_p,
642 c_p / *Chl*, and b_{bp} / *Chl* in the SCM layer (Fig. 9). The b_{bp} / c_p ratio, while at slightly different
643 wavelengths (700 nm and 660 nm, respectively) are at absorption minima and thus this ratio is
644 comparable to the backscattering ratio b_{bp} / b_p. The b_{bp} / b_p ratio is a demonstrated proxy for
645 determining relative constituent composition (Twardowski et al. 2001), with phytoplankton
646 exhibiting lower ratios than nonalgal particles (approximately 0.5% and 1%, respectively; Boss
647 et al. 2004; Whitmire et al. 2007; Westberry et al. 2010). The b_{bp} / *Chl* and c_p / *Chl* ratios are
648 both proxies for the POC / *Chl* ratio (e.g. Claustre et al. 1999; Oubelkheir et al. 2005;
649 Behrenfeld et al. 2015; Álvarez et al. 2016), and thus an indicator of the contribution of
650 phytoplankton to the whole organic carbon pool. The variations are also interpreted as changes
651 in the composition of phytoplankton communities (e.g. Sathyendranath et al. 2009) and their
652 acclimation to the light-nutrient regime (e.g. Geider et al. 1987; Loisel & Morel 1998; Geider
653 et al. 1997; Cloern 1999) if one assumes that nonalgal particles are negligible (e.g., as indicated
654 by the backscattering ratio) or not varying in concentration. The differences between the b_{bp} /
655 *Chl* and c_p / *Chl* ratios lie in the fact that they are sensitive to different particle size ranges
656 (Roesler and Boss 2008) and, thus, when they are not correlated, one can qualitatively discern
657 differing dynamics across the phytoplankton size spectrum.

658 The b_{bp} / c_p ratio is very different between the Ligurian and Ionian Seas, with significantly
659 lower values in the Ligurian Sea (0.0068±0.0009, and 0.0095±0.0009; Fig. 9). These ratios
660 indicate that, in the general sense, the Ligurian Sea SCM is more phytoplankton dominated than

661 the Ionian Sea SCM, which tends towards nonalgal particles. In the Ligurian Sea, the b_{bp} / c_p
662 ratio remains <0.0087 and reaches a minimum of 0.0055 over the period coinciding with the
663 production event from mid-July to mid-August (Fig. 9a), consistent with phytoplankton
664 dominance. In contrast, in the Ionian Sea SCM, the b_{bp} / c_p ratio increases from 0.0085 in late
665 May, peaking at nearly 0.012 in early August, and then decreasing back to 0.0085 in September
666 (Fig. 9b). The tendency towards a ratio of 0.01 (or 1%) in the core of the oligotrophic season,
667 evidences the increased proportion of nonalgal particles to the bulk pool as previously observed
668 in oligotrophic environments (Yentsch & Phinney 1989; Stramski et al. 2004; Loisel et al.
669 2007).

670 The c_p and b_{bp} to *Chl* ratios exhibit not only different temporal patterns between the Ligurian
671 and Ionian Sea SCMs, they also exhibit different relative values. The c_p / *Chl* ratio in the
672 Ligurian Sea SCM is higher than that of the Ionian Sea, ranging from 0.18 to 0.45 m^2 mg Chl^{-1}
673 (mean value of 0.29±0.06 m^2 mg Chl^{-1}), compared to 0.15 to 0.26 m^2 mg Chl^{-1} (mean value
674 of 0.20±0.03 m^2 mg Chl^{-1}), respectively. These results are consistent with the study of Loisel
675 & Morel (1998), reporting low values ranging within 0.1–0.2 m^2 mg Chl^{-1} at the deep
676 chlorophyll maximum level of oligotrophic sites. In contrast, although the b_{bp} / *Chl* ratio in the
677 Ligurian Sea SCM ranges from 0.0011 to 0.0023 m^2 mg Chl^{-1}, and the Ionian Sea from 0.0015
678 to 0.0021 m^2 mg Chl^{-1}, they have essentially identical mean values over the time series
679 (0.0017±0.0006 and 0.0017±0.0001, respectively). The b_{bp} / *Chl* ratio being more sensitive to
680 small-sized particles than the c_p / *Chl* ratio, these results suggest that, in the SCM layer, the
681 POC in the small size fractions of the Ligurian and Ionian Seas is more similar than that in the
682 large size fractions.

683 Temporally, the Ligurian Sea SCM exhibits significantly more temporal variations in both
684 ratios compared to the Ionian Sea SCM, and the temporal variations are highly correlated. Both
685 the c_p / *Chl* and b_{bp} / *Chl* ratios in the Ligurian Sea SCM exhibit a peak at the start of the time

686 series in late May that decreases to mid-July, followed by a second peak during the period
687 coinciding with the production episode from mid-July to mid-August, and then a third increase
688 until the end of the time series (Figs. 9b–c). In contrast, both ratios in the Ionian Sea SCM
689 exhibit significantly reduced temporal variability (Figs. 9e–f), with a weak increase is observed
690 starting in early August.

691 Despite differing temporal variability, the b_{bp} / *Chl* ratio in both Seas remains moderate to
692 low (<0.0025 m^2 mg Chl^{-1}; Figs. 9c and 9f), consistent with global SCM values (Barbieux et
693 al., 2018). The enhanced b_{bp} / *Chl* values observed in the Ligurian Sea SCM in early May, late
694 July and late August suggest an increased contribution of small (pico- and nano-sized)
695 phytoplankton (Cetinić et al. 2012; Cetinić et al. 2015). Yet, the BOUSSOLE pigment data do
696 not reveal pronounced changes in the phytoplankton assemblage. Low-light conditions
697 typically prevailing in the SCM layer are usually associated with low values of the c_p / *Chl* and
698 b_{bp} / *Chl* ratios (e.g. Loisel & Morel 1998; Behrenfeld & Boss 2003; Westberry et al., 2008;
699 Barbieux et al. 2019). These low values may reflect photoacclimation, by which phytoplankton
700 organisms increase their intracellular *Chl*, and/or an increase in the fluorescence-to-*Chl* ratio in
701 relation to limited or null non-photochemical chlorophyll fluorescence quenching.
702 Nevertheless, the temporal variability in the c_p / *Chl* and b_{bp} / *Chl* values may be resulting from
703 fluctuations in the light conditions at the SCM in the Ligurian Sea. In the Ionian Sea, the
704 invariant low c_p / *Chl* and b_{bp} / *Chl* values are consistent with both photoacclimation of
705 phytoplankton to low-light conditions and a diatom-dominated phytoplankton assemblage
706 (Cetinić et al. 2015; Barbieux et al. 2018). The relatively stable ratios observed in this region
707 suggest a relative steadiness in the composition of the phytoplankton assemblage over the
708 considered period.

3.4.2 Relation to abiotic conditions

The Ligurian Sea exhibits enhanced community production during the period from mid-July to mid-August 2014, which is associated with a comparatively moderate increase in the biomass indicators (Figs. 3–4) and c_p-derived POC (Fig. 7a). During this time period, the depth of the SCM shoals by 25 m. This change occurs concurrently with a slight shoaling of the density isopycnals (Figs. 3a–c), and a doubling (from 0.5 to 1 mol quanta m^{-2} d^{-1}) in the daily PAR within the SCM layer (Fig. 10a). Therefore, we suggest that the observed production episode may result from physical forcing that induces an upwelling of the water mass, thereby resulting in an alleviation of the light/nutrient limitation and an adequate balance between light and nutrient availability in the SCM layer. This SCM production episode is associated with a moderate phytoplankton biomass (0.8 Chl mg m^{-3}), dominated by a nanoplankton community. It coincides with an increase in the c_p / *Chl* and b_{bp} / *Chl* ratios, which we attribute to a boost in the carbon-to-*Chl* ratio resulting from production in enhanced light conditions. Because it appears to result from changes in light conditions, we may attribute this production event to photosynthetic (not community) growth.

In the Ionian Sea, the depth of the SCM follows the depth of the isopycnal 28.85 during the period from late to May to mid-August 2017 (Figs. 3d–f). In mid-August, the SCM reaches its deepest point (~125 m) concurrent with deepening isopycnals, decreased PAR levels within the SCM layer (Fig. 10b) and minimum values of *Chl*, c_p and b_{bp}. Afterwards, the SCM depth decouples from the position of the isopycnals (Fig. 3d–f), the SCM becomes shallower and the mean daily PAR in the SCM layer increases. Nevertheless, the observed temporal fluctuations in the abiotic forcing and biological indicators do not seem to relate with any clear change in the community production (Figs. 7d–f). This suggests that physics-induced changes in the position of the SCM are not sufficient to alleviate the light and/or nutrient limitation occurring at this time in the study location (Guieu et al. 2020). Considering the large contribution of

diatoms at the SCM, one may conclude that the low, yet non-negligible, production levels estimated in the SCM layer are supported by diatoms. This result supports previous findings that indicate, contrary to the classic view of diatoms thriving essentially in dynamic eutrophic conditions, these organisms have the ability to maintain in stratified oligotrophic environments, including in deep layers under low light-nutrient conditions (Kemp & Villareal 2013; Kemp & Villareal, 2018). This was also highlighted by Marañón et al. (2021) based on observations in the Mediterranean Sea (PEACETIME cruise).

3.5 Contribution of the SCM to the water column production

In order to assess the relative contribution of the SCM layer to the production occurring in the whole water column, we compare the c_p-based estimates integrated within the productive layer (0–1.5 Z_{eu}) and SCM layers. Our results suggest that, for these oligotrophic systems, the production integrated within the SCM layer represents a substantial fraction (F_{SCM}) of the gross community production integrated within the productive layer. This is particularly the case for the Ligurian Sea where F_{SCM} reaches ~42%, and to a lesser extent for the Ionian Sea with F_{SCM} ~16%.

Subtropical stratified oligotrophic gyres cover 45% of the global ocean (McClain et al. 2004). Assuming that the Ionian Sea is representative of such systems (e.g. Mignot et al. 2014; Barbieux et al. 2019), and extrapolating the estimated relative contribution of the SCM layer to the water column production in the Ionian (F_{SCM} ~16%), then the SCM layer would contribute ~7% of the community production of the water column on a global scale (i.e. F_{SCM} of 16% multiplied by a global spatial occurrence of 45%). In addition, using a global BGC-Argo database, Cornec et al. (2021) estimated that SCMs in oligotrophic subtropical gyres behave as SBM 8–42% of the year, depending on the season. Thus, assuming the Ligurian SCM oligotrophic summer system as a reference for SBM, the contribution of the SCM layer to the

global water column production could seasonally reach 19% (i.e. F_{SCM} of 42% multiplied by a global spatial occurrence of 45%).

We recognize that these estimates are very crude and need to be refined and confirmed in future studies. Yet they suggest that the contribution of the SCM layer to the water column production may be significant globally, although commonly ignored. Our observations are consistent with previous findings in the Mediterranean Sea (Crombet et al. 2011; Marañón et al. 2021) and in other regions of the world ocean (Kemp & Villareal 2013; Mignot et al. 2014), and suggest that stratified oligotrophic systems should no longer be considered as steady oceanic deserts and that their biogeochemical contribution should be accounted for and better quantified to improve global carbon budgets.

4 Conclusions

The present study represents a first attempt to apply the bio-optical diel cycle-based method (Siegel et al. 1989; Claustre et al. 2008) to the c_p and b_{bp} coefficients measured by two BGC-Argo profiling floats. It aims to quantify gross community production in different layers of the water column, the subsurface chlorophyll maximum (SCM) layer in particular, during the oligotrophic summer season in two distinct systems of the Mediterranean, i.e. the Ligurian Sea and the Ionian Sea.

From a methodological point of view, our results indicate that, compared to the c_p coefficient, the diel cycle of the b_{bp} coefficient is not an optimal proxy for the daily POC variations regardless of the water column layer and (Ligurian or Ionian) region under consideration. These results have major implications for use of the methodology with geostationary ocean color missions and standard BGC-Argo profiling floats that yield only the b_{bp} coefficient. The present results thus argue in favor of a frequent implementation onto BGC-Argo floats of transmissometers (c_p sensors), which provide information on a suite of key

biogeochemical variables (Claustre et al. 2020), from phytoplankton community composition (Rembauville et al. 2017), to particle flux export (Briggs et al. 2011; Estapa et al. 2013) and, as demonstrated here, biological production (White et al. 2017; Briggs et al. 2018).

Our c_p-based gross community production rates compare consistently with previous estimates from a similar approach applied to oligotrophic waters (Claustre et al. 2008; Gernez et al. 2011; Barnes & Antoine 2014). Nevertheless, these estimates on average decrease by 25% or increase by 37% depending on the used c_p-to-POC relationship, which is not negligible and raises the question of the selection of an empirical bio-optical relationship for converting c_p into POC equivalent. Hence, we recommend POC sampling simultaneously to BGC-Argo floats deployment. This will help to better constrain bio-optical relationships and ultimately improve the reliability of the biomass and production estimates.

Our results indicate that both the Ligurian and Ionian Seas may sustain relatively large levels of gross community production during the oligotrophic summer period, with a substantial contribution by the SCM layer, a feature characteristic of oligotrophic systems that is typically considered as steady and non-productive. Our results also suggest that the contribution of the SCM layer varies broadly depending the considered system, whether seasonally (Ligurian Sea) or permanently (Ionian) oligotrophic. These results agree with previous BGC-Argo-based studies describing the occurrence and functioning of SCM systems in the global ocean (Mignot et al. 2014; Cornec et al. 2021) and Mediterranean Sea (Lavigne et al. 2015; Barbieux et al. 2019), and offer a first attempt to quantify biological production in such systems.

Our study emphases the promising potential of BGC-Argo profiling floats for providing a non-intrusive, high-frequency assessment of POC production within the whole water column, which is critical in particular for applications to stratified oligotrophic environments with recurring or permanent SCMs. The present results, based on data from two Mediterranean environments, should be confirmed in the future through the deployment of “multi-profiling”

807 BGC-Argo floats in the broad, remote subtropical gyres. In such systems, biological production
808 is not constant but, instead, shows high temporal heterogeneity (Karl et al. 2003; Claustre et al.
809 2008) that may be missed by traditional sampling, leading to a potential underestimate of the
810 biogeochemical impact of these systems in global carbon budgets. Implementing such a BGC-
811 Argo-based approach to carbon flux quantification becomes even more important in the
812 perspective of climate change, which is predicted to induce an expansion of stratified
813 oligotrophic gyres and an oligotrophication of the oceans (Sarmiento et al. 2004) as already
814 observed from satellite imagery (Polovina et al. 2008; Signorini et al. 2015).

815

816 *Author contribution* MB, JU and AB designed the work and prepared the manuscript. MB
817 processed the data and conducted the analyses. MB, JU and CR prepared the plots. AM and BG
818 developed the biological production model. AM helped with the implementation of the model
819 and the interpretation of the output data. CR contributed to the analysis of the diel bio-optical
820 variability, interpretation of bio-optical data and the organization of the manuscript. HC
821 contributed to the interpretation of the BGC-Argo data and biological production. HL helped
822 with the interpretation of the bio-optical data and the global extrapolation of the results. VT and
823 FDO contributed to the BGC-Argo float deployments and interpretation of the physical data.
824 AP prepared and tested the BGC-Argo floats prior to deployment and set up the raw data stream.
825 EL and CP developed the BGC-Argo float version used in this study and contributed to float
826 preparation. CS handled BGC-Argo data archiving and distribution. All authors reviewed and
827 approved the manuscript.

828

829 *Data availability* The BGC-Argo profiling float data and metadata used in this paper may
830 be downloaded from the Argo GDAC (http://doi.org/10.17882/42182). All other original data
831 are available from the Argo Global Data Assembly Center (ftp://ftp.ifremer.fr/ifremer/argo).

These data were collected and made freely available by the International Argo Program and the national programs that contribute to it (http://www.argo.ucsd.edu; https://www.ocean-ops.org). The Argo Program is part of the Global Ocean Observing System. The PEACETIME project pigment data are available from the SEANOE archive under the following reference: Guieu et al., Biogeochemical dataset collected during the PEACETIME cruise, SEANOE, https://doi.org/10.17882/75747, 2020. The BOUSSOLE program pigment data may be accessed upon request (http://www.obs-vlfr.fr/Boussole/html/boussole_data/login_form.php).

Acknowledgement This paper represents a contribution to the following projects: PEACETIME (https://doi.org/10.17600/17000300), a joint initiative of the MERMEX and ChArMEx components supported by CNRS-INSU, IFREMER, CEA, and Météo-France as part of the program MISTRALS coordinated by INSU; PEACETIME-OC supported by the French program CNES-TOSCA; remOcean funded by ERC (grant 246777); and NAOS funded by ANR Equipex (grant J11R107-F). MB was funded by a PhD grant from Sorbonne Université (Ecole Doctorale 129). Phytoplankton pigment analyses were performed at the SAPIGH national HPLC analytical service at the Institut de la Mer de Villefranche (IMEV). We acknowledge the captains and crew of the Téthys and Pourquoi Pas? research vessels during the BOUSSOLE and PEACETIME cruises, as well as David Antoine, PI of the BOUSSOLE project, and Cécile Guieu and Karine Desboeufs, PIs of the PEACETIME project. We thank the International Argo Program and Coriolis project, which contributed to making the data freely and publicly available. Marin Cornec is also warmly thanked for useful discussion regarding biological production in SCM systems. We finally wish to thank the two anonymous Reviewers and the co-Editor-in-Chief for their useful comments and suggestions.

856 **References**

857 Ahn, Y.-H., Bricaud, A., and Morel, A.: Light backscattering efficiency and related properties
858 of some phytoplankters, Deep-Sea Res. Pt. A, 39, 1835–1855,
859 https://doi.org/10.1016/0198-0149(92)90002-B, 1992.

860 Allen, J.I., Somerfield, P.J., and Siddorn, J.: Primary and bacterial production in the
861 Mediterranean Sea: a modelling study, J. Mar. Syst., 33–34, 473–495,
862 https://doi.org/10.1016/S0924-7963(02)00072-6, 2002.

863 Álvarez, E., Morán, X. A. G., López-Urrutia, Á., and Nogueira, E.: Size-dependent
864 photoacclimation of the phytoplankton community in temperate shelf waters (southern
865 Bay of Biscay), Mar. Ecol. Prog. Ser., 543, 73–87, https://doi.org/10.3354/meps11580,
866 2016.

867 Antoine, D., Morel, A., and André, J.-M.: Algal pigment distribution and primary production
868 in the eastern Mediterranean as derived from coastal zone color scanner observations, J.
869 Geophys. Res, 100, 16193–16209, https://doi.org/10.1029/95JC00466, 1995.

870 Antoine, D. André, J.-M, and Morel, A.: Oceanic primary production: 2. Estimation at global
871 scale from satellite (Coastal Zone Color Scanner) chlorophyll, Global Biogeochem. Cy.,
872 10, 57–69, https://doi.org/10.1029/95GB02832, 1996.

873 Antoine, D., D'Ortenzio, F., Hooker, S. B., Bécu, G., Gentili, B., Tailliez, D., and Scott, A. J.:
874 Assessment of uncertainty in the ocean reflectance determined by three satellite ocean
875 color sensors (MERIS, SeaWiFS and MODIS-A) at an offshore site in the Mediterranean
876 Sea (BOUSSOLE project), J. Geophys. Res., 113, 1–22,
877 https://doi.org/10.1029/2007JC004472, 2008.

878 Barber, R. T., and Hitling, A. K.: History of the study of plankton productivity, in:
879 Phytoplankton Productivity: Carbon assimilation in marine and freshwater ecosystems,

880 edited by Williams, P. J. le B., Thomas, D. N., and Reynolds, C. S., Blackwell Science,
881 Oxford, 16–43, https://doi.org/10.1002/9780470995204, 2002.

882 Barbieux, M., Uitz, J., Bricaud, A., Organelli, E., Poteau, A., Schmechtig, C., Gentili, B.,
883 Penkerc'h, C., Leymarie, E., D'Ortenzio, F., and Claustre, H.: Assessing the variability
884 in the relationship between the particulate backscattering coefficient and the chlorophyll
885 a concentration from a global Biogeochemical-Argo database, J. Geophys. Res., 123,
886 1229–1250, https://doi.org/10.1002/2017JC013030, 2017.

887 Barbieux, M., Uitz, J., Gentili, B., Pasqueron de Fommervault, O., Mignot, A., Poteau, A.,
888 Schmechtig, C., Taillandier, V., Leymarie, E., Penkerc'h, C., D'Ortenzio, F., Claustre,
889 H., and Bricaud, A.: Bio-optical characterization of subsurface chlorophyll maxima in the
890 Mediterranean Sea from a Biogeochemical-Argo float database, Biogeosciences, 16,
891 1321–1342, https://doi.org/10.5194/bg-16-1321-2019, 2019.

892 Barnes, M., and Antoine, D.: Proxies of community production derived from the diel variability
893 of particulate attenuation and backscattering coefficients in the northwest mediterranean
894 sea, Limnol. Oceanogr., 59, 2133–2149, https://doi.org/10.4319/lo.2014.59.6.2133,
895 2014.

896 Beckmann, A. and Hense, I.: Beneath the surface: Characteristics of oceanic ecosystems under
897 weak mixing conditions – A theoretical investigation, Prog. Oceanogr., 75, 771–796,
898 https://doi.org/10.1016/j.pocean.2007.09.002, 2007.

899 Behrenfeld, M. J., and Boss, E.: The beam attenuation to chlorophyll ratio: an optical index of
900 phytoplankton physiology in the surface ocean?, Deep-Sea Res. Pt. I, 50, 1537–1549,
901 https://doi.org/10.1016/j.dsr.2003.09.002, 2003.

902 Behrenfeld, M. J., and Boss, E.: Beam attenuation and chlorophyll concentration as alternative
903 optical indices of phytoplankton biomass, J. Mar. Res., 64, 431–451,
904 https://doi.org/10.1357/002224006778189563, 2006.

905 Behrenfeld, M. J., Marañón, E., Siegel, D. A., and Hooker, S. B.: Photoacclimation and
906 nutrient-based model of light-saturated photosynthesis for quantifying oceanic primary
907 production, Mar. Ecol. Prog. Ser., 228, 103–117, https://doi.org/10.3354/meps228103,
908 2002.

909 Bernard, S., Probyn, T. A., and Quirantes, A.: Simulating the optical properties of
910 phytoplankton cells using a two-layered spherical geometry, Biogeosciences Discuss., 6,
911 1497–1563, https://doi.org/10.5194/bgd-6-1497-2009, 2009.

912 Bethoux, J. P., Morin, P., Madec, C., and Gentili, B.: Phosphorus and nitrogen behaviour in the
913 Mediterranean Sea, Deep-Sea Res., 39, 1641–1654, https://doi.org/10.1016/0198-
914 0149(92)90053-V, 1992.

915 Bosc, E., Bricaud, A., and Antoine, D.: Seasonal and interannual variability in algal biomass
916 and primary production in the Mediterranean Sea, as derived from 4 years of SeaWiFS
917 observations, Global Biogeochem. Cy. 18, GB1005,
918 https://doi.org/10.1029/2003GB002034, 2004.

919 Boss, E., Pegau, W. S., Lee, M., Twardowski, M., Shybanov, E., Korotaev, G., and Baratange,
920 F.: Particulate backscattering ratio at LEO 15 and its use to study particle composition
921 and distribution, J. Geophys. Res., 109, C01014, https://doi.org/10.1029/2002JC001514,
922 2004.

923 Boss., E., and Zaneveld, J. R. V.: The effect of bottom substrate on inherent optical properties:
924 Evidence of biogeochemical processes. Limnol. Oceanogr., 48, 346–354.
925 https://doi.org/10.4319/lo.2003.48.1_part_2.0346, 2003.

926 Bricaud, A., Morel, A., and Prieur, L.: Absorption by dissolved organic matter of the sea
927 (yellow substance) in the UV and visible domains, Limnol. Oceanogr., 26,
928 https://doi.org/10.4319/lo.1981.26.1.0043, 1981.

929 Briggs, N., Perry, M. J., Cetinić, I., Lee, C., D'Asaro, E., Gray, A. M., Rehm, E.: High-
930 resolution observations of aggregate flux during a sub-polar North Atlantic spring bloom,
931 Deep-Sea Res. Pt. I, 58, 1031–1039, https://doi.org/10.1016/j.dsr.2011.07.007, 2011.

932 Briggs, N., Guðmundsson, K., Cetinić, I., D'Asaro, E., Rehm, E., Lee, C., and Perry, M. J.: A
933 multi-method autonomous assessment of primary productivity and export efficiency in
934 the springtime North Atlantic, Biogeosciences, 15, 4515–4532,
935 https://doi.org/10.5194/bg-15-4515-2018, 2018.

936 Brunet C., Casotti R., Vantrepotte V., and Conversano F.: Vertical variability and diel dynamics
937 of picophytoplankton in the Strait of Sicily, Mediterranean Sea, in summer, Mar. Ecol.
938 Prog. Ser., 346, 15–26, https://doi.org/10.3354/meps07017, 2007.

939 Brunet, C., Casotti, R., and Vantrepotte, V.: Phytoplankton diel and vertical variability in
940 photobiological responses at a coastal station in the Mediterranean Sea, J Plank Res, 30,
941 645–654, https://doi.org/10.1093/plankt/fbn028, 2008.

942 Casotti, R., Landolfi, A., Brunet, C., D'Ortenzio, F., Mangoni, O., and Ribera d'Alcalá, M.:
943 Composition and dynamics of the phytoplankton of the Ionian Sea (eastern
944 Mediterranean), J. Geophys. Res., 108, 1–19, https://doi.org/10.1029/2002JC001541,
945 2003.

946 Cetinić, I., Perry, M. J., Briggs, N. T., Kallin, E., D'Asaro, E. A., and Lee, C. M.: Particulate
947 organic carbon and inherent optical properties during 2008 North Atlantic Bloom
948 Experiment, J. Geophys. Res., 117, 1–18, https://doi.org/10.1029/2011JC007771, 2012.

949 Cetinić, I., Perry, M. J., D'Asaro, E., Briggs, N., Poulton, N., Sieracki, M. E., and Lee, C. M.:
950 A simple optical index shows spatial and temporal heterogeneity in phytoplankton
951 community composition during the 2008 North Atlantic Bloom Experiment,
952 Biogeosciences, 12, 2179–2194, https://doi.org/10.5194/bg-12- 2179-2015, 2015.

953 Chavez F. P., Messié, M., and Pennington, J. T.: Marine Primary Production in Relation to
954 Climate Variability and Change, Annual Rev. Mar. Sci., 3, 227–260,
955 https://doi.org/10.1146/annurev.marine.010908.163917, 2013.

956 Claustre, H.: The trophic status of various oceanic provinces as revealed by phytoplankton
957 pigment signatures, Limnol. Oceanogr., 39, 1206–1210, 39,
958 https://doi.org/10.4319/lo.1994.39.5.1206, 2014.

959 Claustre, H., Bricaud, A., Babin, M., Bruyant, F., Guillou, L., Le Gall, F., Marie, D., Partensky,
960 F.: Diel variations in Prochlorococcus optical properties, Limnol. Oceanogr., 47, 1637–
961 1647, https://doi.org/10.4319/lo.2002.47.6.1637, 2002.

962 Claustre, H., Huot, Y., Obernosterer, I., Gentili, B., Tailliez, D., and Lewis, M.: Gross
963 community production and metabolic balance in the South Pacific Gyre, using a non
964 intrusive bio-optical method, Biogeosciences, 5, 463–474, https://doi.org/10.5194/bg-5-
965 463-2008, 2008.

966 Cloern, J. E.: The relative importance of light and nutrient limitation of phytoplankton growth:
967 A simple index of coastal ecosystem sensitivity to nutrient enrichment, Aquat. Ecol., 33,
968 3–16, https://doi.org/10.1023/A:1009952125558, 1999.

969 Cornec, M., Claustre, H., Mignot, A., Guidi, L., Lacour, L., Poteau, A., D'Ortenzio, F., Gentili,
970 B., and Schmechtig, C.: Deep chlorophyll maxima in the global ocean: occurrences,
971 drivers and characteristics, Global Biogeochem. Cy., 35, e2020GB006759,
972 https://doi.org/10.1029/2020GB006759, 2021.

973 Corno, G., Letelier, R.M., Abbott, M. R., and Karl, D.M.: Assessing primary production
974 variability in the North Pacific Subtropical Gyre: A comparison of Fast Repetition Rate
975 Fluorometry and ^{14}C measurements, J. Phycol., 42, https://doi.org/10.1111/j.1529-
976 8817.2006.00163.x, 2005.

977 Crombet, Y., Leblanc, K., Quéguiner, B., Moutin, T., Rimmelin, P., Ras, J., Claustre, H.,
978 Leblond, N., Oriol, L., and Pujo-Pay, M.: Deep silicon maxima in the stratified
979 oligotrophic Mediterranean Sea, Biogeosciences, 8, 459–475, https://doi.org/10.5194/bg-
980 8-459-2011, 2011.

981 Cullen, J. J.: The deep chlorophyll maximum: comparing vertical profiles of chlorophyll a, Can.
982 J. Fish. Aquat. Sci., 39, 791–803, https://doi.org/10.1139/f82-108, 1982.

983 Cullen, J. J., Lewis, M. R., Davis, C. O., and Barber, R. T.: Photosynthetic characteristics and
984 estimated growth rates indicate grazing is the proximate control of primary production in
985 the equatorial Pacific, J. Geophys. Res., 97, 639–654,
986 https://doi.org/10.1029/91JC01320, 1992.

987 Cullen, J. J., and Lewis, M. R.: Biological processes and optical measurements near the sea
988 surface: Some issues relevant to remote sensing, J. Geophys. Res., 100(C7), 13255–
989 13266, https://doi.org/10.1029/95JC00454, 1995.

990 Cullen, J. J.: Subsurface chlorophyll maximum layers: enduring enigma or mystery solved?,
991 Ann Rev Mar Sci., 7, 207-39, https://doi.org/10.1146/annurev-marine-010213-135111,
992 2015.

993 Dandonneau, Y.: Measurement of in situ profiles of primary production using an automated
994 sampling and incubation device, ICES Mar. Sci. Sym., 197, 172–180, 1993.

de Boyer Montégut, C., Madec, G., Fischer, A. S., Lazar, A., and Iudicone, D.: Mixed layer depth over the global ocean: An examination of profile data and a profile-based climatology, J. Geophys. Res., 109, 1–20, https://doi.org/10.1029/2004JC002378, 2004.

del Giorgio P. A., and Duarte C. M.: Respiration in the open ocean, Nature, 420, 37984. https://doi.org/10.1038/nature01165, 2002.

Di Cicco, A., Sammartino, M, Marullo, S., and Santoleri, R.: Regional empirical algorithms for an improved identification of phytoplankton functional types and size classes in the Mediterranean Sea using satellite data, Frontiers Mar. Sci., 4126, 1–18, https://doi.org/ 10.3389/fmars.2017.00126, 2017.

D'Ortenzio, F. and Ribera d'Alcalà, M.: On the trophic regimes of the Mediterranean Sea: a satellite analysis, Biogeosciences, 6, 139–148, https://doi.org/10.5194/bg-6-139-2009, 2009.

Duarte, C. M., and Agusti S.: The CO_2 balance of unproductive aquatic ecosystems, Science, 281, 234–6, https://doi.org/10.1126/science.281.5374.234, 1998.

Dubinsky, Z., and Stambler, N.: Photoacclimation processes in phytoplankton: mechanisms, consequences, and applications, Aquat. Microb. Ecol., 56,163–176, https://doi.org/10.3354/ame01345, 2009.

Dugdale, R. C., and Wilkerson, F. P.: Nutrient sources and primary production in the Eastern Mediterranean, Oceanologica Acta, 1988.

Durand, M. D., and Olson, R. J.: Contributions of phytoplankton light scattering and cell concentration changes to diel variations in beam attenuation in the equatorial pacific from flow cytometric measurements of pico-, ultra and nanoplankton, Deep-Sea Res. Pt. II, 43, 891–906, https://doi.org/10.1016/0967-0645(96)00020-3, 1996.

1018 Durand, M. D., and Olson, R.J.: Diel patterns in optical properties of the chlorophyte
1019 Nannochloris sp.: Relating individual-cell to bulk measurements, Limnol. Oceanogr., 43,
1020 1107–1118, https://doi.org/10.4319/lo.1998.43.6.1107, 1998.

1021 Durand, M. D. Green, R. E., Sosik, H. M. and Olson, R. J.: Diel Variations in Optical Properties
1022 of Micromonas Pusilla (Prasinophyceae), J. Phycol., 38, 1132–1142,
1023 https://doi.org/10.1046/j.1529-8817.2002.02008.x, 2002.

1024 Estapa, M. L., Buesseler, K., Boss, E., and Gerbi, G.: Autonomous, high-resolution
1025 observations of particle flux in the oligotrophic ocean, Biogeosciences, 10, 5517–5531,
1026 https://doi.org/10.5194/bg-10-5517-2013, 2013.

1027 Falkowski, P. G.: Ocean Science: The power of plankton, Nature, 483**,** S17–S20,
1028 https://doi.org/10.1038/483S17a, 2012.

1029 Fennel, K., and Boss, E.: Subsurface maxima of phytoplankton and chlorophyll: Steady-state
1030 solutions from a simple model, Limnol. Oceanogr., 48, 1521–1534,
1031 https://doi.org/10.4319/lo.2003.48.4.1521, 2003.

1032 Field, C. B., Behrenfeld, M. J., Randerson, J. T., and Falkowski, P.: Primary production of the
1033 biosphere: integrating terrestrial and oceanic components, Science 281, 237–240,
1034 https://doi.org/10.1126/science.281.5374.237, 1998.

1035 Fitzwater, S.E., Knauer, G.A., and Martin, J.H.: Metal contamination and its effect on primary
1036 production measurements, Limnol. Oceanogr., 27, 44–551,
1037 https://doi.org/10.4319/lo.1982.27.3.0544, 1982.

1038 Gardner, W. D., Mishonov, A. V., and Richardson, M. J.: Global POC concentrations from in-
1039 situ and satellite data, Deep-Sea Res. Pt. II, 53, 718-740,
1040 https://doi.org/10.1016/j.dsr2.2006.01.029, 2006.

1041 Geider, R. J.: Light and temperature dependence of the carbon to chlorophyll a ratio in
1042 microalgae and cyanobacteria: Implications for physiology and growth of phytoplankton,
1043 New Phytol., 106, 1–34, https://doi.org/10.1111/j.1469-8137.1987.tb04788.x, 1987.

1044 Geider, R. J., MacIntyre, H. L., and Kana T. M.: Dynamic model of phytoplankton growth and
1045 acclimation: Responses of the balanced growth rate and the chlorophyll a:carbon ratio to
1046 light, nutrient-limitation and temperature, Mar. Ecol. Prog. Ser., 148, 187–200,
1047 https://doi.org/10.3354/meps148187, 1997.

1048 Gernez, P., Antoine, D., and Huot, Y.: Diel cycles of the particulate beam attenuation
1049 coefficient under varying trophic conditions in the northwestern Mediterranean Sea:
1050 Observations and modeling, Limnol. Oceanogr., 56, 17–36,
1051 https://doi.org/10.4319/lo.2011.56.1.0017, 2011.

1052 Gitelson, A., Karnieli, A., Goldman, N., Yacobi, Y.Z., and Mayo, M.: Chlorophyll estimation
1053 in the Southeastern Mediterranean using CZCS images: adaptation of an algorithm and
1054 its validation, J. Mar. Syst., 9, 283–290, https://doi.org/10.1016/S0924-7963(95)00047-
1055 X, 1996.

1056 Guieu, C., D'Ortenzio, F., Dulac, F., Taillandier, V., Doglioli, A., Petrenko, A., Barrillon, S.,
1057 Mallet, M., Nabat, P., and Desboeufs, K.: Introduction: Process studies at the air–sea
1058 interface after atmospheric deposition in the Mediterranean Sea – objectives and strategy
1059 of the PEACETIME oceanographic campaign (May–June 2017), Biogeosciences, 17,
1060 5563–5585, https://doi.org/10.5194/bg-17-5563-2020, 2020.

1061 González, N., Anadón, R., Mouriño, B., Fernández, E., Sinha, B., Escánez, J., and de Armas,
1062 D.: The metabolic balance of the planktonic community in the North Atlantic Subtropical
1063 Gyre: The role of mesoscale instabilities, Limnol. Oceanogr., 4,
1064 https://doi.org/10.4319/lo.2001.46.4.0946, 2001.

González, N., Anadón, R., and Marañón, E.: Large-scale variability of planktonic net community metabolism in the Atlantic Ocean: Importance of temporal changes in oligotrophic subtropical waters, Mar. Ecol. Progr. Ser., 233, 21–30, https://doi.org/10.3354/meps233021, 2002.

Gordon, H. R., and McCluney, W. R.: Estimation of the Depth of Sunlight Penetration in the Sea for Remote Sensing, Appl. Opt., 14, 413–416, https://doi.org/10.1364/AO.14.000413, 1975.

Hense, I., and Beckmann, A.: Revisiting subsurface chlorophyll and phytoplankton distributions, Deep-Sea Res. Pt. I, 55, 1193–1199, https://doi.org/10.1016/j.dsr.2008.04.009, 2008.

Jacquet, S., Lennon, J.-F., Marie, D., and Vaulot, D.: Picoplankton population dynamics in coastal waters of the northwestern Mediterranean Sea, Limnol. Oceanogr., 43, 1916–1931, https://doi.org/10.4319/lo.1998.43.8.1916, 1998.

Juranek, L. W., and Quay, P. D.: In vitro and in situ gross primary and net community production in the North Pacific Subtropical Gyre using labeled and natural abundance isotopes of dissolved O_2, Glob. Biogeochem. Cy., 19, https://doi.org/10.1029/2004GB002384, 2005.

Karl, D. M., Laws, E. A., Morris, P., Williams, P. J. le B, and Emerson, S.: Metabolic balance of the open sea, Nature, 426, 32–32, https://doi.org/10.1038/426032a, 2003.

Kemp, A. E. S., and Villareal, T. A.: High diatom production and export in stratified waters - A potential negative feedback to global warming, Prog. Oceanogr., 119, 4–23, https://doi.org/10.1016/j.pocean.2013.06.004, 2013.

1087 Kemp, A. E. S., and Villareal, T. A.: The case of the diatoms and the muddled mandalas: Time
1088 to recognize diatom adaptations to stratified waters, Prog. Oceanogr., 167, 138-149,
1089 https://doi.org/10.1016/j.pocean.2018.08.002, 2018.

1090 Kheireddine, M., and Antoine, D.: Diel variability of the beam attenuation and backscattering
1091 coefficients in the northwestern Mediterranean Sea (BOUSSOLE site), J. Geophys. Res.,
1092 119, 5465– 5482, https://doi.org/10.1002/2014JC010007, 2014.

1093 Kiefer, D. A., Olson, R. J., and Holm-Hansen, O.: Another look at the nitrite and chlorophyll
1094 maxima in the central North Pacific, Deep-Sea Res., 23, 1199–1208,
1095 https://doi.org/10.1016/0011-7471(76)90895-0, 1976.

1096 Kolber, Z. S., and Falkowski, P. G.: Use of active fluorescence to estimate phytoplankton
1097 photosynthesis in-situ, Limnol. Oceanogr., 38, 1646–1665, 1993.

1098 Lacroix, G., and Nival, P.: Influence of meteorological variability on primary production
1099 dynamics in the Ligurian Sea (NW Mediterranean Sea) with a 1D
1100 hydrodynamic/biological model, J. Mar. Syst., 16, 23–50, https://doi.org/10.1016/S0924-
1101 7963(97)00098-5, 1998.

1102 Lavigne, H., D'Ortenzio, F., Migon, C., Claustre, H., Testor, P., Ribera d'Alcalà, M., Lavezza,
1103 R., Houpert, L., and Prieur, L.: Enhancing the comprehension of mixed layer depth
1104 control on the Mediterranean phytoplankton phenology, J. Geophys. Res. Oceans, 118,
1105 3416–3430, https://doi.org/10.1002/jgrc.2025, 2013.

1106 Lavigne, H., D'Ortenzio, F., Ribera D'Alcalà, M., Claustre, H., Sauzède, R., and Gacic, M.: On
1107 the vertical distribution of the chlorophyll a concentration in the Mediterranean Sea: a
1108 basin-scale and seasonal approach, Biogeosciences, 12, 5021–5039,
1109 https://doi.org/10.5194/bg-12-5021-2015, 2015.

1110 Letelier, R. M., Karl, D. M., Abbott, M. R., Bidigare, R. R.: Light driven seasonal patterns of
1111 chlorophyll and nitrate in the lower euphotic zone of the North Pacific Subtropical Gyre,
1112 Limnol. Oceanogr., 2, 508–519, https://doi.org/10.4319/lo.2004.49.2.0508, 2004.

1113 Litaker, R.W., Warner, V., Rhyne, C.F., Duke, C.S., Kenney, B.E., Ramus, J., and Tester, P.A.:
1114 Effect of diel and interday variations in light on the cell division pattern and in situ growth
1115 rates of the bloom-forming dinoflagellate Heterocapsa triquetra, *Mar Ecol Prog Ser, 232*,
1116 63–74, https://doi.org/10.3354/MEPS232063, 2002.

1117 Loisel, H., Mériaux, X., Berthon, J.-F., Poteau, A.: Investigation of the optical backscattering
1118 to scattering ratio of marine particles in relation to their biogeochemical composition in
1119 the eastern English Channel and southern North Sea, Limnol. Oceanogr., 52, 739–752,
1120 https://doi.org/10.4319/lo.2007.52.2.0739, 2007.

1121 Loisel, H., Vantrepotte, V., Norkvist, K., Mériaux, X., Kheireddine, M., Ras, J., Pujo-Pay, M.,
1122 Combet, Y., Leblanc, K., Dall'Olmo, G., Mauriac, R., Dessailly, D., and Moutin, T.:
1123 Characterization of the bio-optical anomaly and diurnal variability of particulate matter,
1124 as seen from scattering and backscattering coefficients, in ultra-oligotrophic eddies of the
1125 Mediterranean Sea, Biogeosciences, 8, 3295–3317, https://doi.org/10.5194/bg-8-3295-
1126 2011, 2011.

1127 Longhurst, A., Sathyendranath, S., Platt, T., and Caverhill, C.: An estimate of global primary
1128 production in the ocean from satelite radiometer data, J. Plank. Res., 17, 1245–1271,
1129 https://doi.org/10.1093/plankt/17.6.1245, 1995.

1130 Magazzu, G., and Decembrini, F.: Primary production, biomass and abundance of phototrophic
1131 picoplankton in the Mediterranean Sea: A review, Aquat. Microb. Ecol., 9, 97– 104,
1132 https://doi.org/10.3354/ame009097, 1995.

1133 Marañón, E., Van Wambeke, F., Uitz, J., Boss, E. S., Dimier, C., Dinasquet, J., Engel, A.,
1134 Haëntjens, N., Pérez-Lorenzo, M., Taillandier, V., and Zäncker, B.: Deep maxima of
1135 phytoplankton biomass, primary production and bacterial production in the
1136 Mediterranean Sea, Biogeosciences, 18, 1749–1767, https://doi.org/10.5194/bg-18-1749-
1137 2021, 2021.

1138 Marra, J., Langdon, C., and Knudson, C. A.: Primary production, water column changes, and
1139 the demise of a Phaeocystis bloom at the Marine Light-Mixed Layers site (59°N, 21°W)
1140 in the northeast Atlantic Ocean, J. Geophys. Res., 100, 6633–6643,
1141 https://doi.org/10.1029/94JC01127, 1995.

1142 Marty, J. C., Chiavérini, J., Pizay, M. D., and Avril, B.: Seasonal and interannual dynamics of
1143 nutrients and phytoplankton pigments in the western Mediterranean Sea at the
1144 DYFAMED time- series station (1991–1999), Deep-Sea Res. Pt. II, 49, 1965–1985,
1145 https://doi.org/10.1016/S0967-0645(02)00022-X, 2002.

1146 Marty, J. C. and Chiavérini, J.: Hydrological changes in the Ligurian Sea (NW Mediterranean,
1147 DYFAMED site) during 1995–2007 and biogeochemical consequences, Biogeosciences,
1148 7, 2117–2128, https://doi.org/10.5194/bg-7-2117-2010, 2010.

1149 Mayot, N., D'Ortenzio, F., Ribera d'Alcalà, M., Lavigne, H., and Claustre, H.: Interannual
1150 variability of the Mediterranean trophic regimes from ocean color satellites,
1151 Biogeosciences, 13, 1901–1917, https://doi.org/10.5194/bg-13-1901-2016, 2016.

1152 McClain, C. R., Signorini, S. R., and Christian, J. R.: Subtropical gyre variability observed by
1153 ocean-color satellites, Deep-Sea Res. Pt. II, 51, 281–301,
1154 https://doi.org/10.1016/j.dsr2.2003.08.002, 2004.

1155 McGillicuddy Jr., D. J.: Mechanisms of Physical-Biological-Biogeochemical Interaction at the
1156 Oceanic Mesoscale, Annu. Rev. Mar. Sci., 8–1, 125–159, 2016.

1157 Mignot, A., Claustre, H., Uitz, J., Poteau, A., D'Ortenzio, F., and Xing, X.: Understanding the
1158 seasonal dynamics of phytoplankton biomass and the deep chlorophyll maximum in
1159 oligotrophic environments: A Bio-Argo float investigation, Global Biogeochem. Cy., 28,
1160 856– 876, https://doi.org/10.1002/2013GB004781, 2014.

1161 Minas, H. J.: La distribution de l'oxygène en relation avec la production primaire en
1162 Méditerranée Nord-Occidentale, Mar. Biol., 7, 181–204,
1163 https://doi.org/10.1007/BF00367489, 1970.

1164 Morel, A.: Light and marine photosynthesis: a spectral model with geochemical and
1165 climatological implications, Prog. Oceanogr., 26, 263–306, https://doi.org/10.1016/0079-
1166 6611(91)90004-6, 1991.

1167 Morel, A., and André, J.-M.: Pigment distribution and primary production in the western
1168 Mediterranean as derived and modeled from coastal zone color scanner observations, J.
1169 Geophys. Res., 96, 12685– 12698, https://doi.org/10.1029/91JC00788, 1991.

1170 Morel, A., Antoine, D., Babin, M., and Dandonneau, Y.: Measured and modeled primary
1171 production in the northeast Atlantic (EUMELI JGOFS program): the impact of natural
1172 variations in photosynthetic parameters on model predictive skill, Deep-Sea Res. Pt. I,
1173 43, 1273–1304, https://doi.org/10.1016/0079-6611(91)90004-6, 1996.

1174 Moutier, W., Duforêt-Gaurier, L., Thyssen, M., Loisel, H., Mériaux, X., Courcot, L., Dessailly,
1175 D., Rêve, M.-H., Grégori, G., Alvain, S., Barani, A., Brutier, L., and Dugrnne, M.:
1176 Evolution of the scattering properties of phytoplankton cells from flow cytometry
1177 measurements, PLOS ONE, 12, e0181180,
1178 https://doi.org/10.1371/journal.pone.0181180, 2017.

1179 Neukermans, G., Loisel, H., Mériaux, X., Astoreca, R., and McKee, D.: In situ variability of
1180 mass-specific beam attenuation and backscattering of marine particles with respect to

particle size, density, and composition, Limnol. Oceanogr., 57, 124–144, https://doi.org/10.4319/lo.2012.57.1.0124, 2012.

Nielsen, E. S.: The Use of radio-active carbon (C^{14}) for measuring organic production in the sea, ICES J. Mar. Sci., 18, 117–140, https://doi.org/10.1093/icesjms/18.2.117, 1952.

Organelli, E., Barbieux, M., Claustre, H., Schmechtig, C., Poteau, A., Bricaud, A., Boss, E., Briggs, N., Dall'Olmo, G., D'Ortenzio, F., Leymarie, E., Mangin, A., Obolensky, G., Penkerc'h, C., Prieur, L., Roesler, C., Serra, R., Uitz, J., and Xing, X.: Two databases derived from BGC-Argo float measurements for marine biogeochemical and bio-optical applications, Earth Syst. Sci. Data, 9, 861–880, https://doi.org/10.5194/essd-9-861-2017, 2017.

Organelli, E., Dall'Olmo, G., Brewin, R. J. W., Taran, G., Boss, E., and Bricaud, A.: The open-ocean missing backscattering is in the structural complexity of particles, Nat. Commun., 9, 5439, https://doi.org/10.1038/s41467-018-07814-6, 2018.

Oubelkheir, K., Claustre, H., Sciandra, A., and Babin, M.: Bio-optical and biogeochemical properties of different trophic regimes in oceanic waters, Limnol. Oceanogr., 50, 1795–1809, https://doi.org/10.4319/lo.2005.50.6.1795, 2015.

Oubelkheir, K. and, Sciandra, A.: Diel variations in particle stocks in the oligotrophic waters of the Ionian Sea (Mediterranean), J. Mar. Syst., 74, 1–2, https://doi.org/10.1016/j.jmarsys.2008.02.008, 2008.

Pasqueron de Fommervault, O., Migon, C., D'Ortenzio, F., Ribera d'Alcalà, M, and Coppola, L.: Temporal variability of nutrient concentrations in the northwestern Mediterranean Sea (DYFAMED time-series station), Deep-Sea Res. Pt. I, 100, 1–12, https://doi.org/10.1016/j.dsr.2015.02.006, 2015.

1204 Polovina, J. J., Howell, E. A., and Abecassis, M.: Ocean's least productive waters are
1205 expanding, Geophys. Res. Lett., 35, L03618, https://doi.org/10.1029/2007GL031745,
1206 2008.

1207 Quay, P. D., Peacock, C., Björkman, K., and Karl, D. M.: Measuring primary production rates
1208 in the ocean: Enigmatic results between incubation and non-incubation methods at Station
1209 ALOHA, Glob. Biogeochem. Cy., 24, https://doi.org/10.1029/2009GB003665, 2010.

1210 Ras, J., Claustre, H., and Uitz, J.: Spatial variability of phytoplankton pigment distributions in
1211 the Subtropical South Pacific Ocean: comparison between in situ and predicted data,
1212 Biogeosciences, 5, 353–369, https://doi.org/10.5194/bg-5-353-2008, 2008.

1213 Regaudie-de-Gioux, A., Lasternas, S., Agustí, S., and Duarte, C. M.: Comparing marine
1214 primary production estimates through different methods and development of conversion
1215 equations, Frontiers, 1, https://doi.org/10.3389/fmars.2014.00019, 2014.

1216 Roesler, C. S. and Boss, E.: In Situ Measurement of the Inherent Optical Properties (IOPs) and
1217 Potential for Harmful Algal Bloom Detection and Coastal Ecosystem Observations. *In*
1218 Babin, M., Roesler, C. S. and Cullen, J. J., Real-time coastal observing systems for marine
1219 ecosystem dynamics and harmful algal blooms: Theory, instrumentation and modelling.
1220 UNESCO, 2008.

1221 Roesler, C., Uitz, J., Claustre, H., Boss, E., Xing, X., Organelli, E., Briggs, N., Bricaud, A.,
1222 Schmechtig, C., Poteau, A., D'Ortenzio, F., Ras, J., Drapeau, S., Haëntjens, N. and
1223 Barbieux, M.: Recommendations for obtaining unbiased chlorophyll estimates from in
1224 situ chlorophyll fluorometers: A global analysis of WET Labs ECO sensors, Limnol.
1225 Oceanogr.-Meth., 15, 572–585, https://doi.org/10.1002/lom3.10185, 2017.

1226 Saba, V.S., Friedrichs, M. A. M., Carr, M.-E., et al.: Challenges of modeling depth-integrated
1227 marine primary productivity over multiple decades: A case study at BATS and HOT,
1228 Glob. Biogeochem. Cy., 24, doi: 10.1029/2009GB003655, 2010.

1229 Saba, V. S., Friedrichs, M. A. M., Antoine, D., Armstrong, R. A., Asanuma, I., Behrenfeld, M.
1230 J., Ciotti, A. M., Dowell, M., Hoepffner, N., Hyde, K. J. W., Ishizaka, J., Kameda, T.,
1231 Marra, J., Mélin, F., Morel, A., O'Reilly, J., Scardi, M., Smith Jr., W. O., Smyth, T. J.,
1232 Tang, S., Uitz, J., Waters, K., and Westberry, T. K.: An evaluation of ocean color model
1233 estimates of marine primary productivity in coastal and pelagic regions across the globe,
1234 Biogeosciences, 8, 489–503, https://doi.org/10.5194/bg-8-489-2011, 2011.

1235 Sarmiento, J. L., and Siegenthaler, U.: New production and the global carbon cycle, in: Primary
1236 productivity and biogeochemical cycles in the sea, Environmental Science Research, vol.
1237 43, edited by Falkowski, P. G., Woodhead A. D., and Vivirito K., Springer, Boston, MA,
1238 https://doi.org/10.1007/978-1-4899-0762-2_18, 1992.

1239 Sarmiento, J. L., Slater, R., Barber, R., Bopp, L., Doney, S. C., Hirst, A. C., Kleypas, J., Matear,
1240 R., Mikolajewicz, U., Monfray, P., Soldatov, V., Spall, S. A., and Stouffer, R.: Response
1241 of ocean ecosystems to climate warming, Global Biogeochem. Cy., 18, 1–23,
1242 https://doi.org/10.1029/2003GB002134, 2014.

1243 Sathyendranath, S., Longhurst, A., Caverhill, C. M., and Platt, T.: Regionally and Seasonally
1244 Differentiated Primary Production in the North Atlantic, Deep-Sea Res. Pt. I, 42, 1773–
1245 1802, https://doi.org/10.1016/0967-0637(95)00059-F, 1995.

1246 Sathyendranath, S., Stuart, V., Nair, A., Oka, K., Nakane, T., Bouman, H., Forget, M.-H.,
1247 Maass, H., and Platt, T.: Carbon-to-chlorophyll ratio and growth rate of phytoplankton in
1248 the sea, Mar. Ecol. Prog. Ser., 383, 73–84, https://doi.org/10.3354/meps07998: 2009.

1249 Schmechtig, C., Poteau, A., Claustre, H., D'Ortenzio, F., and Boss, E.: Processing Bio-Argo
1250 chlorophyll a concentration at the DAC Level, Argo Data Management, 1–22,
1251 https://doi.org/10.13155/39468, 2015.

1252 Schmechtig, C., Poteau, A., Claustre, H., D'Ortenzio, F., Dall'Olmo, G., and Boss, E.:
1253 Processing Bio-Argo particle backscattering at the DAC level Version, Argo Data
1254 Management, 1–13, https://doi.org/10.13155/39459, 2016.

1255 Serret, P., Fernandez, E., Sostres, J. A., and Anadon, R.: Seasonal compensation of microbial
1256 production and respiration in a temperate sea, Mar. Ecol. Prog. Ser., 187, 43–57,
1257 https://doi.org/10.3354/meps187043, 1999.

1258 Siegel, D. A., Dickey, T.D., Washburn, L., Hamilton, M. K., and Mitchell, B. G: Optical
1259 determination of particulate abundance and production variations in the oligotrophic
1260 ocean, Deep-Sea Res. Pt. A, 36, 211–222, https://doi.org/10.1016/0198-0149(89)90134-
1261 9, 1989.

1262 Signorini, S. R., Franz B. A., and McClain C. R.: Chlorophyll variability in the oligotrophic
1263 gyres: mechanisms, seasonality and trends, Frontiers Mar. Sci., 2,
1264 https://doi.org/10.3389/fmars.2015.00001, 2015.

1265 Siokou-Frangou, I., Christaki, U., Mazzocchi, M. G., Montresor, M., Ribera d'Alcalá, M.,
1266 Vaqué, D., and Zingone, A.: Plankton in the open Mediterranean Sea: a review,
1267 Biogeosciences, 7, 1543–1586, https://doi.org/10.5194/bg-7-1543-2010, 2010.

1268 Slade, W. H., and Boss, E.: Spectral attenuation and backscattering as indicators of average
1269 particle size, Applied Opt., 54, 7264–7277, http://dx.doi.org/10.1364/AO.54.007264,
1270 2015.

1271 Smyth, T. J., Pemberton, K. L. , Aiken, J., and Geider, R. J.: A methodology to determine
1272 primary production and phytoplankton photosynthetic parameters from Fast Repetition Rate

1273 Fluorometry, J. Plank. Res., 26, 11, 1337–1350, https://doi.org/10.1093/plankt/fbh124,
1274 2004.

1275 Stramska, M., and Dickey, T. D.: Variability of bio-optical properties of the upper ocean
1276 associated with diel cycles in phytoplankton population, J. Geophys. Res., 97, 17873–
1277 17887, https://doi.org/10.1029/92JC01570, 1992.

1278 Stramski, D., and Kiefer, D.A.: Light scattering by microorganisms in the open ocean. Prog.
1279 Oceanogr., 28, 343–383, https://doi.org/10.1016/0079-6611(91)90032-H, 1991.

1280 Stramski, D., and Reynolds, R. A.: Diel variations in the optical properties of a marine diatom.
1281 Limnol. Oceanogr., 38, 1347–1364, https://doi.org/10.4319/lo.1993.38.7.1347, 1993.

1282 Stramski, D., Reynolds, R. A., Kahru, M., and Mitchell, B. G.: Estimation of particulate organic
1283 carbon in the ocean from satellite remote sensing, Science, 285, 239–242,
1284 https://doi.org/10.1126/science.285.5425.239, 1999.

1285 Stramski, D., Bricaud, A., and Morel, A.: Modeling the inherent optical properties of the ocean
1286 based on the detailed composition of the planktonic community, Appl. Opt., 40, 2929–
1287 2945, https://doi.org/10.1364/AO.40.002929, 2001.

1288 Stramski, S., Boss, E., Bogucki, D., and Voss., K. J.: The role of seawater constituents in light
1289 backscattering in the ocean, Prog. Oceanogr., 61, 27–56,
1290 https://doi.org/10.1016/j.pocean.2004.07.001, 2004.

1291 Stramski, D., Reynolds, R. A., Babin, M., Kaczmarek, S., Lewis, M. R., Röttgers, R., Sciandra,
1292 A., Stramska, M., Twardowski, M. S., Franz, B. A., and Claustre, H.: Relationships
1293 between the surface concentration of particulate organic carbon and optical properties in
1294 the eastern South Pacific and eastern Atlantic Oceans, Biogeosciences, 5, 171–201,
1295 https://doi.org/10.5194/bg-5-171-2008, 2008.

1296 Suggett, D. J., Macintyre, H. L., and Geider, R. J.: Evaluation of biophysical and optical
1297 determinations of light absorption by photosystem II in phytoplankton, Limnol. Oceanogr.
1298 Methods, 316–332, https://doi.org/10.4319/lom.2004.2.316, 2004.

1299 Sullivan, J., Twardowski, M., Ronald, S., Zaneveld, J. V., and Moore, C. C.: Measuring optical
1300 backscattering in water, in: Light scattering reviews, edited by Kokhanovsky, A. A.,
1301 Springer, Berlin, 7, 189–224, 2013.

1302 Taillandier, V., Wagener, T., D'Ortenzio, F., Mayot, N., Legoff, H., Ras, J., Coppola, L.,
1303 Pasqueron de Fommervault, O., Schmechtig, C., Diamond, E., Bittig, H., Lefevre, D.,
1304 Leymarie, E., Poteau, A., and Prieur, L.: Hydrography and biogeochemistry dedicated to
1305 the Mediterranean BGC-Argo network during a cruise with RV Tethys 2 in May 2015,
1306 Earth Syst. Sci. Data, 10, 627–641, https://doi.org/10.5194/essd-10-627-2018, 2018.

1307 Turley, C. M., Bianchi, M., Christaki, U., Conan, P., Harris, J. R. W., Psarra, S., Ruddy, G.,
1308 Stutt, E. D., Tselepides, A., Van Wambeke, F.: Relationship between primary producers
1309 and bacteria in an oligotrophic sea - The Mediterranean and biogeochemical implications,
1310 Mar. Ecol. Progr. Ser., 193, 11–18, https://doi.org/10.3354/meps193011, 2000.

1311 Twardowski, M. S., Boss, E., Macdonald, J. B., Pegau, W. S., Barnard, A. H., and Zaneveld, J.
1312 R. V.: A model for estimating bulk refractive index from the optical backscattering ratio
1313 and the implications for understanding particle composition in case I and case II waters.
1314 J. Geophys. Res., 106, 14129–14142, https://doi.org/10.1029/2000JC000404, 2001.

1315 Uitz, J., Claustre, H., Morel, A., and Hooker, S. B.: Vertical distribution of phytoplankton
1316 communities in open ocean: An assessment based on surface chlorophyll, J. Geophys.
1317 Res., 111, 1–23, https://doi.org/10.1029/2005JC003207, 2006.

1318 Uitz, J., Claustre, H., Gentili, B., and Stramski, D.: Phyto- plankton class-specific primary
1319 production in the world's oceans: Seasonal and interannual variability from satellite

observations, Global Biogeochem. Cy., 24, 1–19, https://doi.org/10.1029/2009gb003680, 2010.

Uitz, J., Stramski, D., Gentili, B., D'Ortenzio, F., and Claustre, H.: Estimates of phytoplankton class-specific and total primary production in the Mediterranean Sea from satellite ocean color observations, Global Biogeochem. Cy., 26, 1–10, https://doi.org/10.1029/2011gb004055, 2012.

Ulloa, O., Sathyendranath, S., and Platt, T.: Effect of the particle-size distribution on the backscattering ratio in seawater, Appl. Opt., 33, 7070–7077, https://doi.org/10.1364/AO.33.007070, 1994.

Vaulot, D., and Marie, D.: Diel variability of photosynthetic picoplankton in the equatorial Pacific, J. Geophys. Res., 104, 3297–3310, https://doi.org/10.1029/98JC01333, 1999.

Vidussi, F., Claustre, H., Manca, B. B., Luchetta, A., and Marty, J.-C.: Phytoplankton pigment distribution in relation to upper thermocline circulation in the eastern Mediterranean Sea during winter, J. Geophys. Res., 106, 19,939-19,956, https://doi.org/10.1029/1999JC000308, 2001.

Westberry, T., Behrenfeld, M. J., Siegel, D. A., and Boss, E.: Carbon-based primary productivity modeling with vertically resolved photoacclimation, Global Biogeoch. Cy., 222, 1–18, https://doi.org/10.1029/2007GB003078, 2008.

Westberry, T. K. Dall'Olmo, G., Boss, E., Behrenfeld, M., and Moutin, T.: Coherence of particulate beam attenuation and backscattering coefficients in diverse open ocean environments, Opt. Express, 18, 15,419–15,425, https://doi.org/10.1364/OE.18.015419, 2010.

White, A. E., Barone, B., Letelier, R. M., and Karl, D. M.: Productivity diagnosed from the diel cycle of particulate carbon in the North Pacific Subtropical Gyre, Geophys. Res. Lett., 44, 3752– 3760, https://doi.org/10.1002/2016GL071607, 2017.

Whitmire, A. L., Boss, E., Cowles, T. J., and Pegau, W. S.: Spectral variability of the particulate backscattering ratio, Opt. Express 15, 7019–7031, https://doi.org/10.1364/OE.15.007019, 2007.

Williams, P. J. le B., and Jenkinson, N.W.: A transportable microprocessor controlled precise Winkler titration suitable for field station and shipboard use, Limnol. Oceanogr., 27, 576–584, https://doi.org/10.4319/lo.1982.27.3.0576, 1982.

Williams, P. J. le B., and Purdie, D. A.: In vitro and in situ derived rates of gross production, net community production and respiration of oxygen in the oligotrophic subtropical gyre of the North Pacific Ocean, Deep-Sea Res. Pt. A, 38, 891–910, https://doi.org/10.1016/0198-0149(91)90024-A, 1991.

Williams, P. J. le B.: On the definition of plankton production terms, in: Measurement of primary production from the molecular to the global scale, edited by Li, W. K., and Maestrini, S. I., ICES mar. Sei. Symp, Copenhagen, 9–19, 1993.

Williams, P. J. le B., Morris, P. J., and Karl, D. M.: Net community production and metabolic balance at the oligotrophic ocean site, station ALOHA, Deep-Sea Res. Pt. I, 51, 1563–1578, https://doi.org/10.1016/j.dsr.2004.07.001., 2004.

Xing, X., Claustre, H., Blain, S., D'Ortenzio, F., Antoine, D., Ras, J., Guinet, C.: Quenching correction for in vivo chlorophyll fluorescence acquired by autonomous platforms: A case study with instrumented elephant seals in the Kerguelen region (Southern Ocean), Limnol. Oceanogr.-Meth., 10, 483–495, https://doi.org/10.4319/lom.2012.10.483, 2012.

1365 Yentsch, C. S., and Phinney, D. A.: A bridge between ocean optics and microbial ecology.
1366 Limnol. Oceanogr., 34, 1694–1705, https://doi.org/10.4319/lo.1989.34.8.1694, 1989.
1367 Zhang, X., Hu, L., and He, M.-X.: Scattering by pure seawater: Effect of salinity, Opt. Express,
1368 17, 5698–5710, https://doi.org/10.1364/OE.17.005698, 2009.

Figure captions

Figure 1: Trajectories of the two BGC-Argo profiling floats fLig (WMO6901776) and fIon (WMO6902828) deployed respectively in the Ligurian Sea (green) and the Ionian Sea (blue), superimposed onto a 9-km resolution summer climatology of surface chlorophyll *a* concentration (in mg m^{-3}) derived from MODIS Aqua ocean color measurements. The asterisk-shaped symbol indicates the geographic location of the BOUSSOLE site.

Figure 2: Schematic representation of the diel variations of the depth-integrated bio-optical properties converted to POC biomass (B) and the sampling strategies employed in the (a) Ligurian Sea and (b) Ionian Sea. The diamond-shaped symbols indicate schematically the float profile times, labeled with time stamps associated with sunrise (sr), noon (n), sunset (ss) and midnight (m), with the corresponding POC biomass estimated within the considered layer (e.g., $B(t_{sr})$, etc.). The numeric subscripts (+1, +2, +4 or +5) indicate the number of days since the first profile of the summertime time series.

Figure 3: Time series of the vertical distribution of the *Chl* (a and d), b_{bp} (b and e), c_p (d and f), and instantaneous midday PAR (d and h), in the Ligurian Sea (left) and the Ionian Sea (right). The euphotic depth (Z_{eu}; white line), the Mixed Layer Depth (MLD; black line), the depth of the SCM (magenta line), and the depth of the isopycnal 28.85 expressed as σ_t (blue line), are superimposed onto the bio-optical timeseries. The dashed lines indicate the dates at which the c_p and the b_{bp} values in the SCM layer reach a minimum.

Figure 4: Temporal evolution of *Chl* (a and d), c_p (b and e), and b_{bp} (c and f) in the surface (dark green) and SCM (red) layers for the Ligurian Sea (left) and the Ionian Sea (right). The dashed lines indicate the dates when the values of c_p and b_{bp} in the SCM layer reach a minimum.

Figure 5: Example of the variations of the c_p (a) and b_{bp} (b) coefficients at the daily time scale in the Ionian Sea in the SCM layer during the interval from September 2 to September 6, 2017. The grey shaded area indicates the nighttime.

Figure 6: Comparison of the biological production integrated within the euphotic layer, derived from the diel cycle of c_p (blue) or b_{bp} (yellow) or computed using the bio-optical primary production model of Morel (1991) (purple) for the Ligurian Sea (a) and the Ionian Sea (b).

Figure 7: Temporal evolution of the POC and community production derived from the diel cycle of c_p in the Ligurian Sea (a–b) and the Ionian Sea (c–d) and integrated in three different

layers of the water column: surface (dark green), euphotic (light blue) and SCM (red) layers. The dotted lines indicate the dates when c_p in the SCM layer reaches a minimum.

Figure 8: Depth-interpolated timeseries of the relative contributions (%) to the chlorophyll *a* concentration of the micro- (a and d), nano- (b and e) and picophytoplankton (c and h) derived from HPLC pigment determinations in the Ligurian Sea (BOUSSOLE site; left) and Ionian Sea (PEACETIME cruise; right). The pigment data were collected at the BOUSSOLE site in the same region and at the same time period as the fLig float deployment (see text section 2.1). The fIon float was deployed concurrently to sampling for HPLC pigments at the PEACETIME ION station. Pigment data collected at ION over four days prior to float deployment are shown. As an indication, the depths of the euphotic depth (Z_{eu}; white dashed line), mixed layer (MLD; black dashed line) and SCM (magenta dashed line) derived from the BGC-Argo float measurements, as in Fig. 3, are overlaid onto the pigment data.

Figure 9: Temporal evolution of the bio-optical ratios of b_{bp} / c_p (a), c_p / *Chl* (b) and b_{bp} / *Chl* (c) in the SCM layer for the Ligurian Sea (left) and the Ionian Sea (right). The dotted lines indicate the dates when the values of c_p in the SCM layer reach a minimum.

Figure 10: Time series of the daily-integrated photosynthetically available radiation (PAR) at the SCM level in the Ligurian Sea (a) and the Ionian Sea (b). The horizontal grey line shows the median of each time series. The dotted lines indicate the dates at which the values of c_p in the SCM layer reach a minimum.

Table 1: POC-to-c_p relationships from the literature, with POC and c_p in units of mg m^{-3} and m^{-1}, respectively.

Reference	Region	Relationship
Marra et al. (1995)	North Atlantic	POC = 367 $c_p(660)$ + 31.2
Claustre et al. (1999)	Equatorial Pacific	POC = 501.81 $c_p(660)$ + 5.33
Oubelkheir et al. (2005)	Mediterranean	POC = 574 $c_p(555)$ – 7.4
Behrenfeld & Boss (2006)	Equatorial Pacific	POC = 585.2 $c_p(660)$ + 7.6
Gardner et al. (2006)	Global Ocean	POC = 381 $c_p(660)$ + 9.4
Stramski et al. (2008)	Pacific and Atlantic, including upwelling	POC = 661.9 $c_p(660)$ – 2.168
Loisel et al (2011)	Mediterranean	POC = 404 $c_p(660)$ + 29.25
Cetinić et al. (2012)	North Atlantic	POC = 391 $c_p(660)$ – 5.8

Table 2: POC-to-b_{bp} relationships from the literature, with POC and b_{bp} in units of mg m^{-3} and m^{-1}, respectively.

Reference	Region	Relationship
Stramski et al. (2008)	Pacific and Atlantic, including upwelling	POC = 71002 $b_{bp}(555)$ – 5.5
Loisel et al (2011)	Mediterranean	POC = 37550 $b_{bp}(555)$ + 1.3
Cetinić et al. (2012)	North Atlantic	POC = 35422 $b_{bp}(700)$ – 14.4

Table 3: Mean and range (%) in relative daily variations ($\widetilde{m\Delta}$ and $\widetilde{r\Delta}$, respectively) in the diel cycle of c_p and b_{bp} computed for each float over the entire time series, for the two considered regions and in the surface (0-Z_{pd}) and SCM layers of the water column.

		Surface layer		**SCM layer**	
Region		$\tilde{\Delta}\boldsymbol{c_p}$	$\tilde{\Delta}\boldsymbol{b_{bp}}$	$\tilde{\Delta}\boldsymbol{c_p}$	$\tilde{\Delta}\boldsymbol{b_{bp}}$
Ligurian Sea	$\widetilde{m\Delta}$	12.7	-2.3	14.5	3.8
	$\widetilde{r\Delta}$	256.7	28.5	194.8	107.8
Ionian Sea	$\widetilde{m\Delta}$	0.55	0.23	1.16	0.06
	$\widetilde{r\Delta}$	54.4	21.2	102.4	57.3

Table 4: Estimates of primary and community production (in units of gC m^{-2} d^{-1}) from the literature in areas of the Mediterranean Sea comparable, when possible, to the considered study regions.

Primary production					
Method	**Reference**	**Area**	**Period**	**Layer**	**Estimate**
Ocean color-coupled bio-optical model	Morel & André (1991)	Western basin	1981	0–Z_{eu}	0.26
	Antoine et al. (1995)	Whole basin	1979-1981	0–1.5Z_{eu}	0.34
	Bosc et al. (2004)	Western basin	1998-2001	0–1.5Z_{eu}	0.45
	-	Eastern basin	-	-	0.33
	Uitz et al. (2012)	Bloom region	May-Aug 1998-2007	0–1.5Z_{eu}	0.26–0.82
	-	No bloom region	-	-	0.22–0.69
Biogeochemical model	Lacroix & Nival (1998)	Ligurian Sea		0–200 m	0.13
	Allen et al. (2002)	Ligurian Sea		0–Z_{eu}	0.33
	-	Ionian Sea		-	0.14
In-situ ^{14}C measurements	Minas (1970)	Northwestern basin	1961-1965	Surface	0.21
	Magazzu & Decembrini (1995)	Ionian Sea	1983-1992	0–Z_{eu}	0.22
	Turley et al. (2000)	Ligurian Sea	Oct 1997, Apr-May 1998	0–Z_{eu}	0.5
	Marañón et al. (2021)	Ionian Sea	May 2017	0–200 m	0.19

Gross community production					
Method	**Reference**	**Area**	**Period**	**Layer**	**Estimate**
c_p diel cycle-based method	Barnes & Antoine (2014)	Ligurian Sea	May-Aug 2006-2011	0–Z_{eu}	0.8–1.5

Table 5: Comparison of the mean rates ± SD (gC m^{-2} d^{-1}) of the community production integrated within the euphotic layer, derived from the application of the bio-optical diel cycle-based method to the c_p measurements, using different bio-optical relationships from the literature for converting the c_p values into POC biomass.

Reference	Ligurian Sea	Ionian Sea
Marra et al. (1995)	0.89±0.84	0.35±0.09
Claustre et al. (1999)	1.22±1.16	0.48±0.12
Oubelkheir et al. (2005)	1.18±1.13	0.46±0.11
Behrenfeld & Boss (2006)	1.43±1.35	0.56±0.14
Gardner et al. (2006)	0.93±0.88	0.36±0.09
Stramski et al. (2008)	1.62±1.54	0.63±0.16
Loisel et al. (2011)	0.98±0.92	0.38±0.10
Cetinić et al. (2012)	0.96±0.91	0.37±0.09

Table 6: Community production mean rates ± SD (gC m^{-2} d^{-1}) derived from the application of the bio-optical diel cycle-based method to the c_p measurements in the two considered regions. The production rates are integrated within the surface, subsurface maximum (SCM), and euphotic layers.

Variable	Ligurian Sea			Ionian Sea		
	Euphotic	Surface	SCM	Euphotic	Surface	SCM
POC (gC m^{-2} d^{-1})	3.67±1.11	0.36±0.17	3.86 ± 1.20	1.88 ±0.24	0.34±0.14	0.93±0.31
GCP (gC m^{-2} d^{-1})	1.18±1.13	0.29±0.33	0.96±1.28	0.46±0.11	0.11±0.04	0.14± 0.39

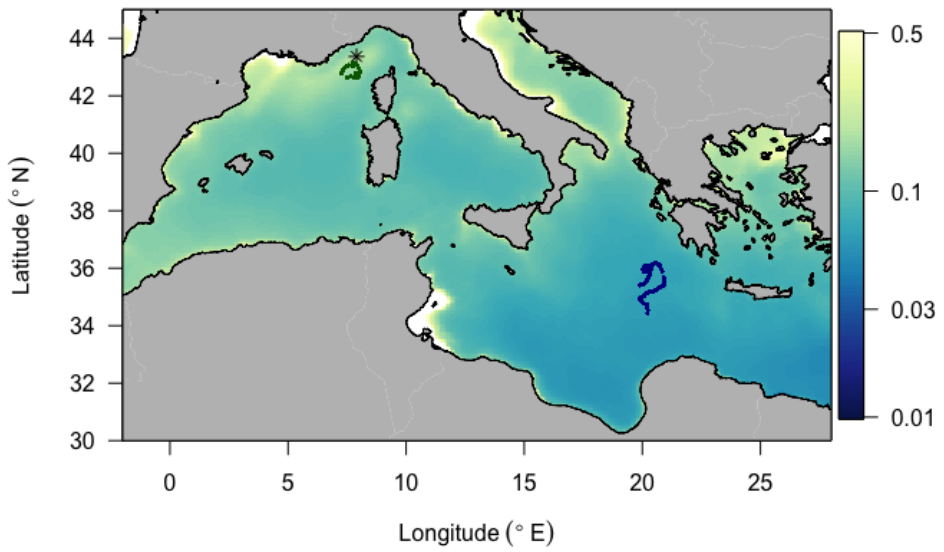

Figure 1: Trajectories of the two BGC-Argo profiling floats fLig (WMO6901776) and fIon (WMO6902828) deployed respectively in the Ligurian Sea (green) and the Ionian Sea (blue), superimposed onto a 9-km resolution summer climatology of surface chlorophyll *a* concentration (in mg m^{-3}) derived from MODIS Aqua ocean color measurements. The asterisk-shaped symbol indicates the geographic location of the BOUSSOLE site.

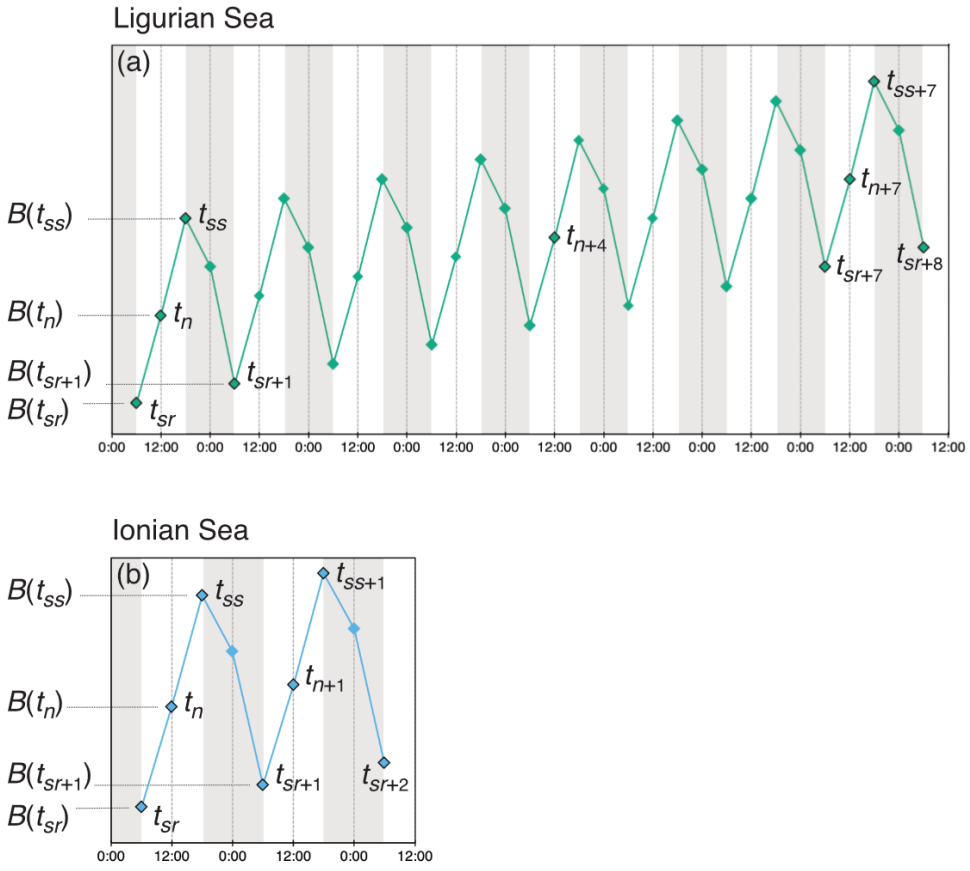

Figure 2: Schematic representation of the diel variations of the depth-integrated bio-optical properties converted to POC biomass (B) and the sampling strategies employed in the (a) Ligurian Sea and (b) Ionian Sea. The diamond-shaped symbols indicate schematically the float profile times, labeled with time stamps associated with sunrise (sr), noon (n), sunset (ss) and midnight (m), with the corresponding POC biomass estimated within the considered layer (e.g., $B(t_{sr})$, etc.). The numeric subscripts (+1, +2, +4 or +5) indicate the number of days since the first profile of the summertime time series.

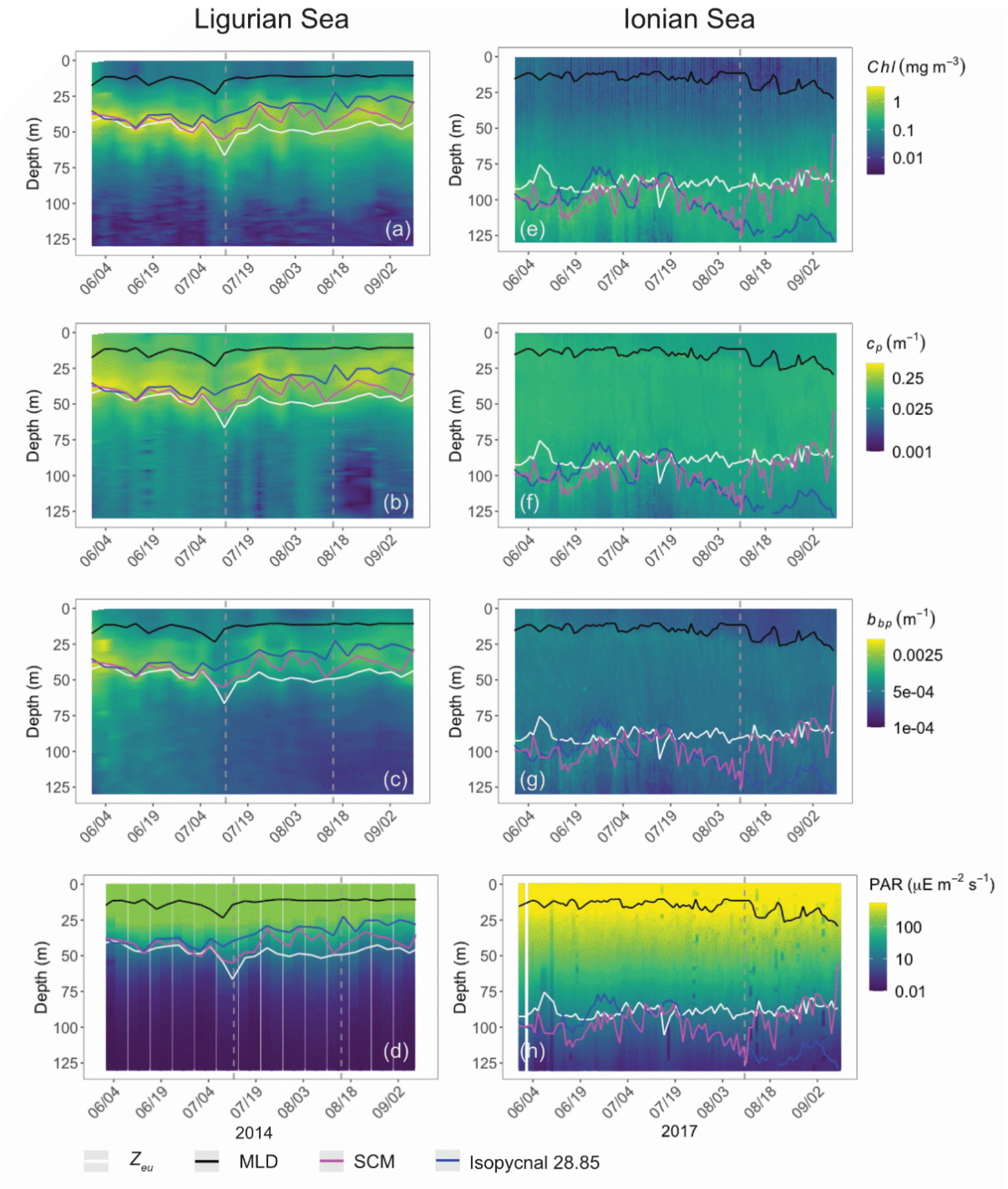

Figure 3: Time series of the vertical distribution of the *Chl* (a and d), b_{bp} (b and e), c_p (d and f), and instantaneous midday PAR (d and h), in the Ligurian Sea (left) and the Ionian Sea (right). The euphotic depth (Z_{eu}; white line), the Mixed Layer Depth (MLD; black line), the depth of the SCM (magenta line), and the depth of the isopycnal 28.85 expressed as (blue line), are superimposed onto the bio-optical timeseries. The dashed lines indicate the dates at which the c_p and the b_{bp} values in the SCM layer reach a minimum.

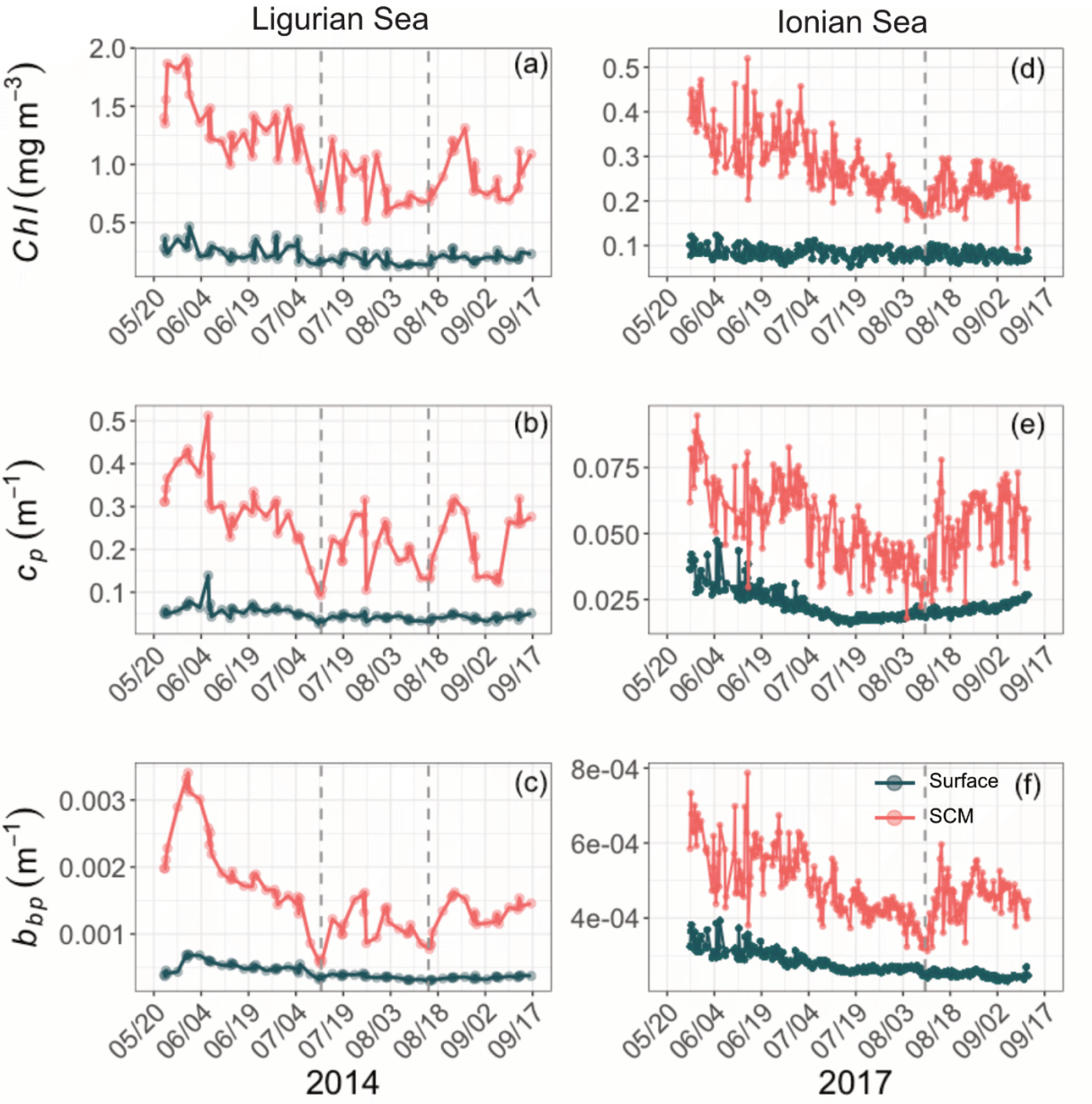

Figure 4: Temporal evolution of *Chl* (a and d), c_p (b and e), and b_{bp} (c and f) in the surface (dark green) and SCM (red) layers for the Ligurian Sea (left) and the Ionian Sea (right). The dashed lines indicate the dates when the values of c_p and b_{bp} in the SCM layer reach a minimum.

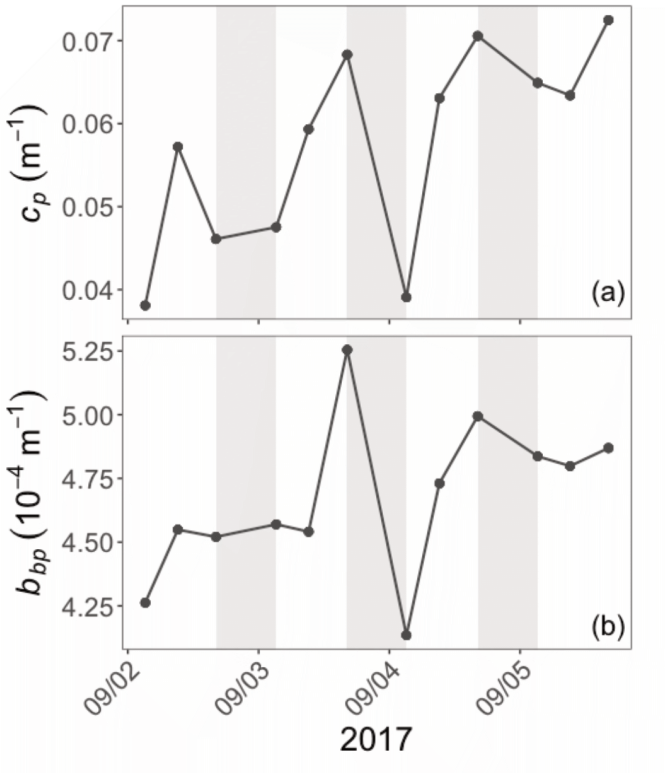

Figure 5: Example of the variations of the c_p (a) and b_{bp} (b) coefficients at the daily time scale in the Ionian Sea in the SCM layer during the interval from September 2 to September 6, 2017. The grey shaded area indicates the nighttime.

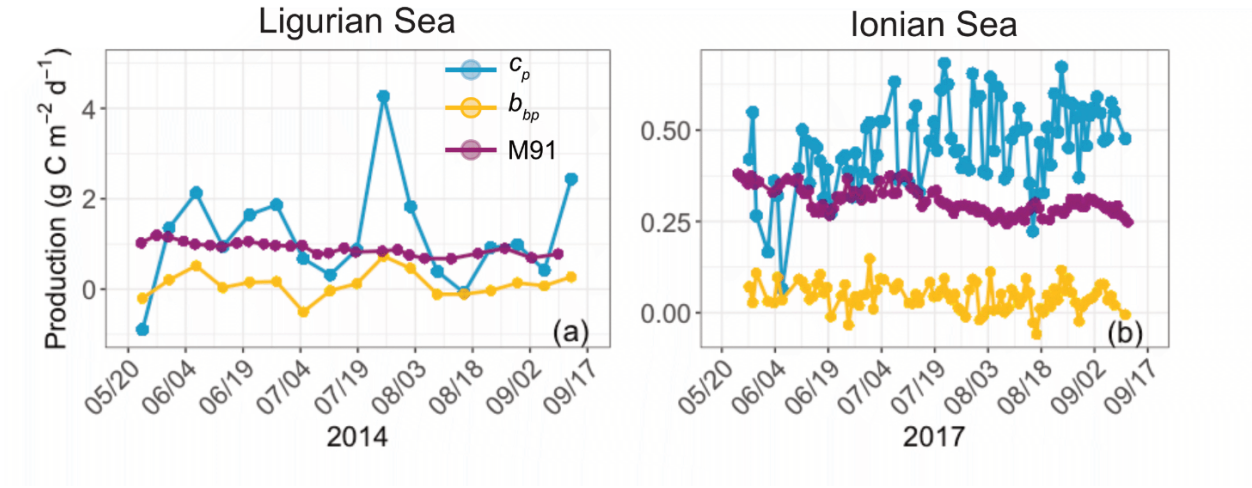

Figure 6: Comparison of the biological production integrated within the euphotic layer, derived from the diel cycle of c_p (blue) or b_{bp} (yellow) or computed using the bio-optical primary production model of Morel (1991) (purple) for the Ligurian Sea (a) and the Ionian Sea (b).

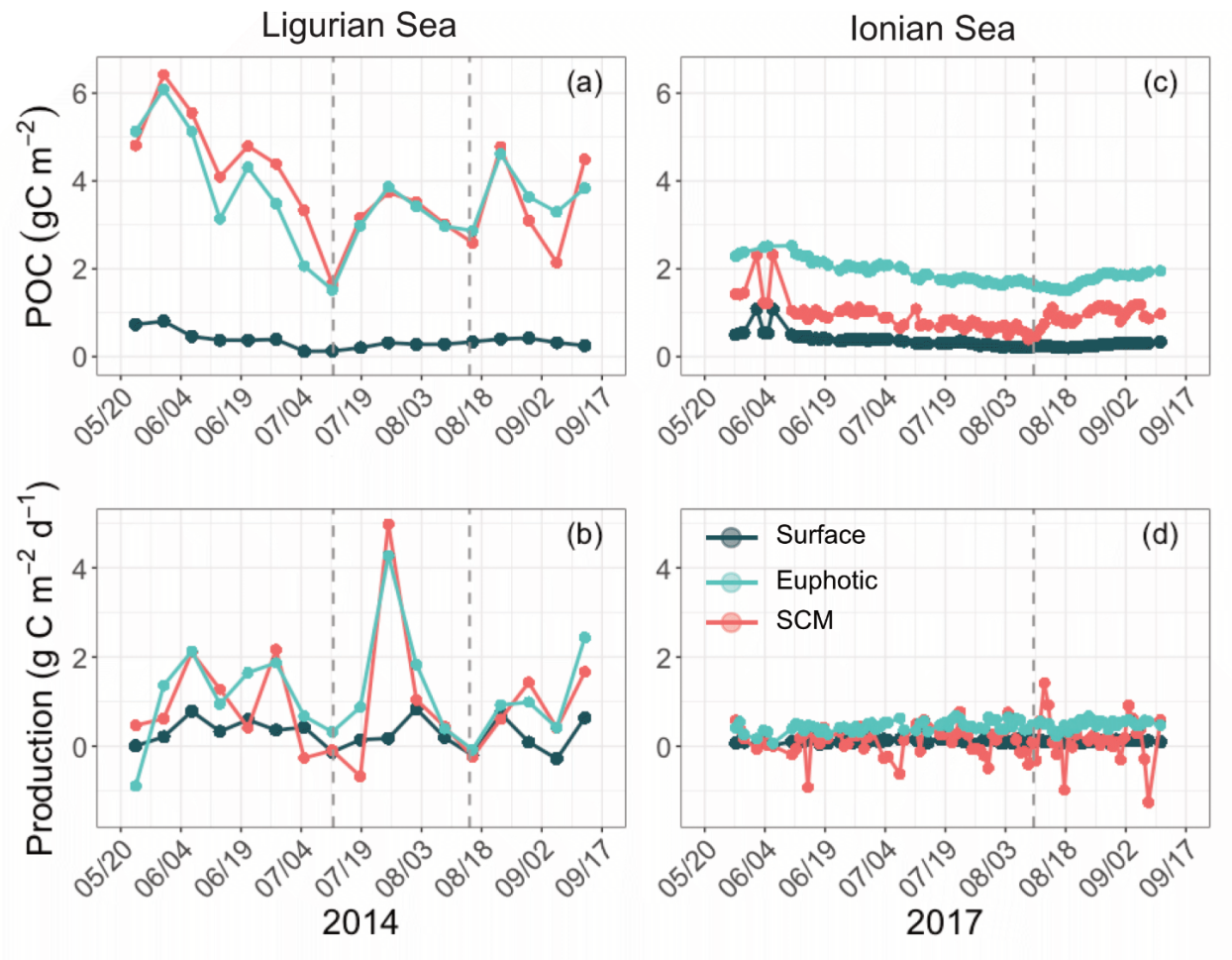

Figure 7: Temporal evolution of the POC and community production derived from the diel cycle of c_p in the Ligurian Sea (a–b) and the Ionian Sea (c–d) and integrated in three different layers of the water column: surface (dark green), euphotic (light blue) and SCM (red) layers. The dotted lines indicate the dates when c_p in the SCM layer reaches a minimum.

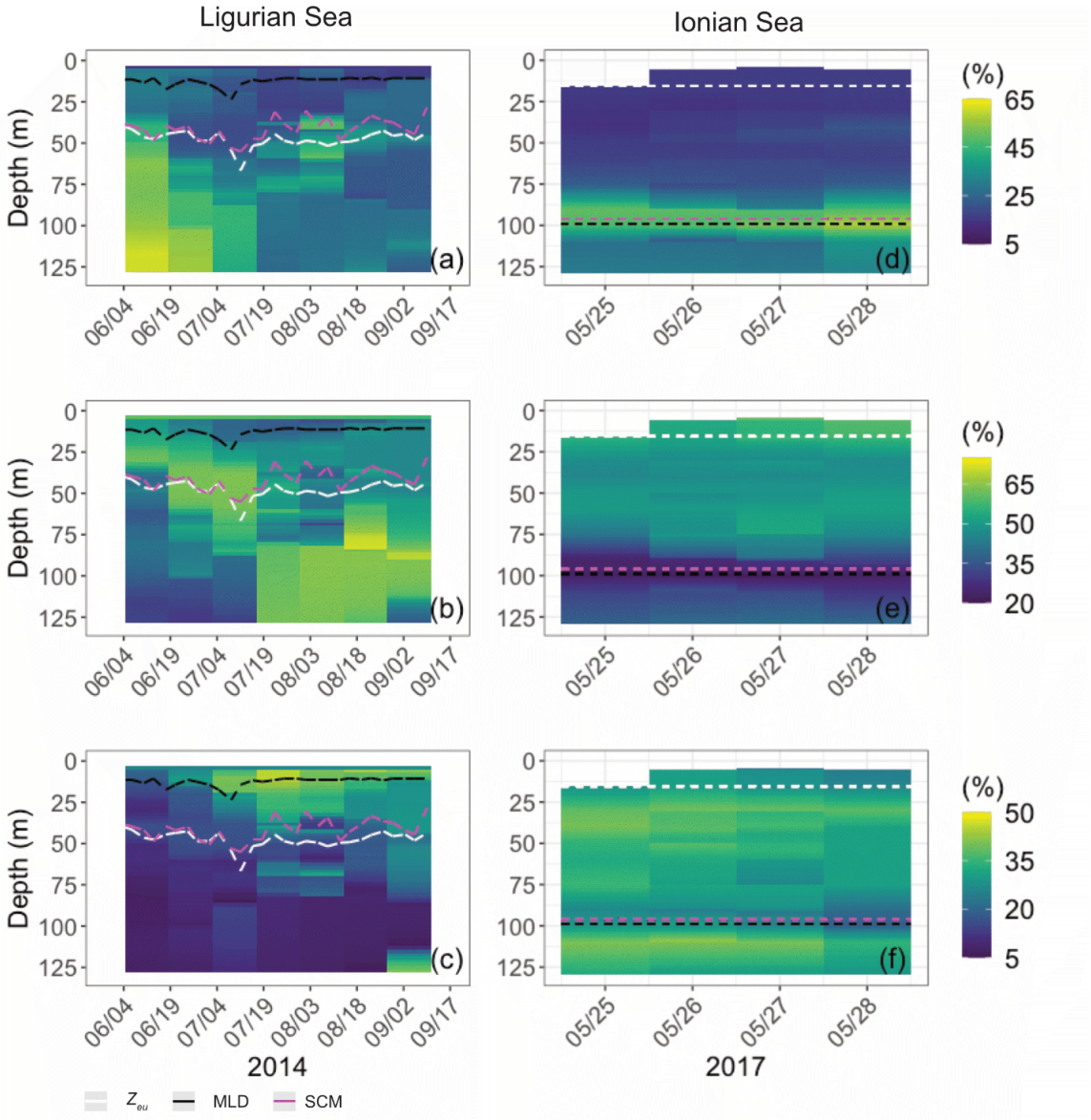

Figure 8: Depth-interpolated timeseries of the relative contributions (%) to the chlorophyll *a* concentration of the micro- (a and d), nano- (b and e) and picophytoplankton (c and h) derived from HPLC pigment determinations in the Ligurian Sea (BOUSSOLE site; left) and Ionian Sea (PEACETIME cruise; right). The pigment data were collected at the BOUSSOLE site in the same region and at the same time period as the fLig float deployment (see text section 2.1). The fIon float was deployed concurrently to sampling for HPLC pigments at the PEACETIME ION station. Pigment data collected at ION over four days prior to float deployment are shown. As an indication, the depths of the euphotic depth (Z_{eu}; white dashed line), mixed layer (MLD; black dashed line) and SCM (magenta dashed line) derived from the BGC-Argo float measurements, as in Fig. 3, are overlaid onto the pigment data.

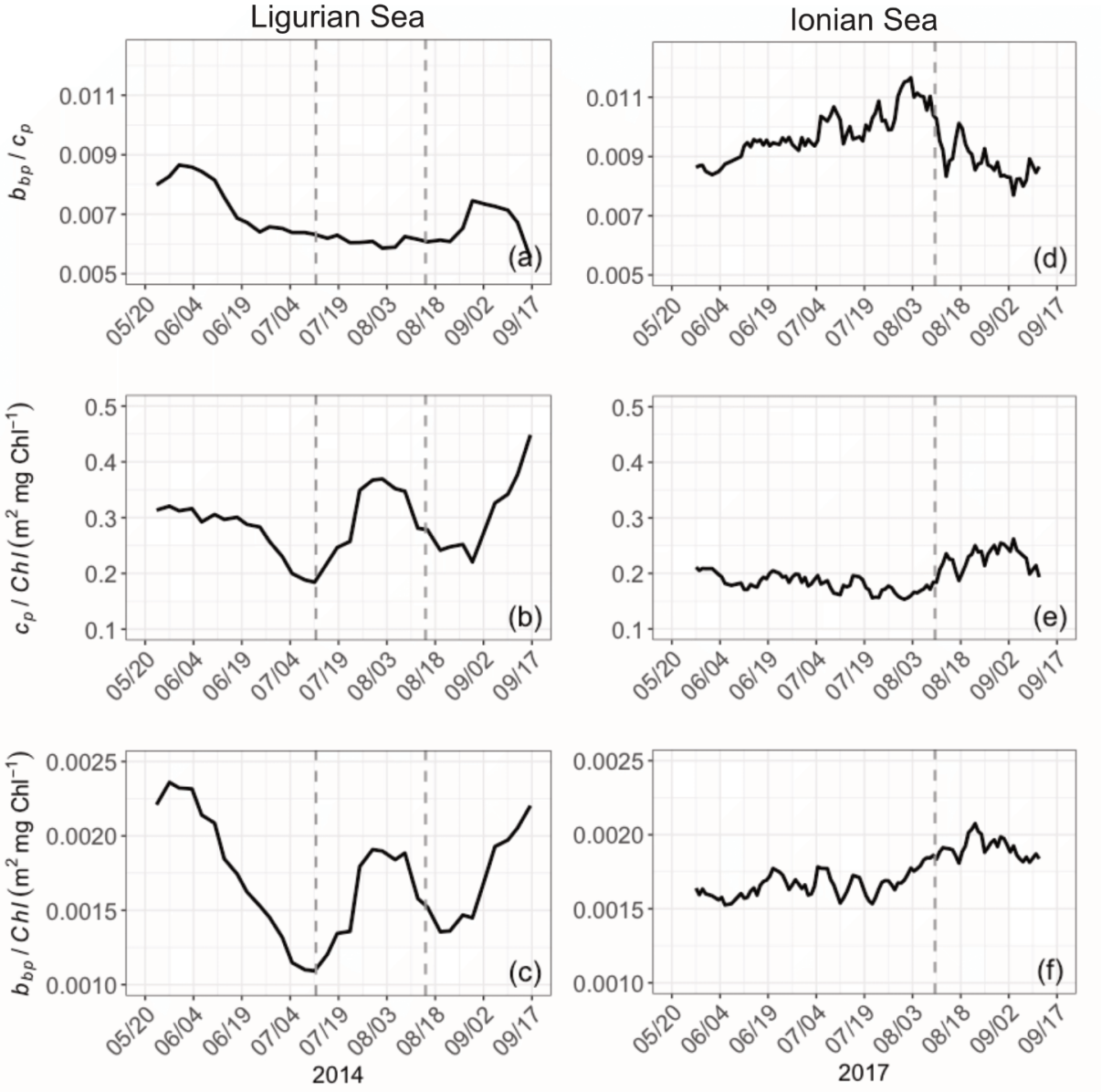

Figure 9: Temporal evolution of the bio-optical ratios of b_{bp} / c_p (a), c_p / *Chl* (b) and b_{bp} / *Chl* (c) in the SCM layer for the Ligurian Sea (left) and the Ionian Sea (right). The dotted lines indicate the dates when the values of c_p in the SCM layer reach a minimum.

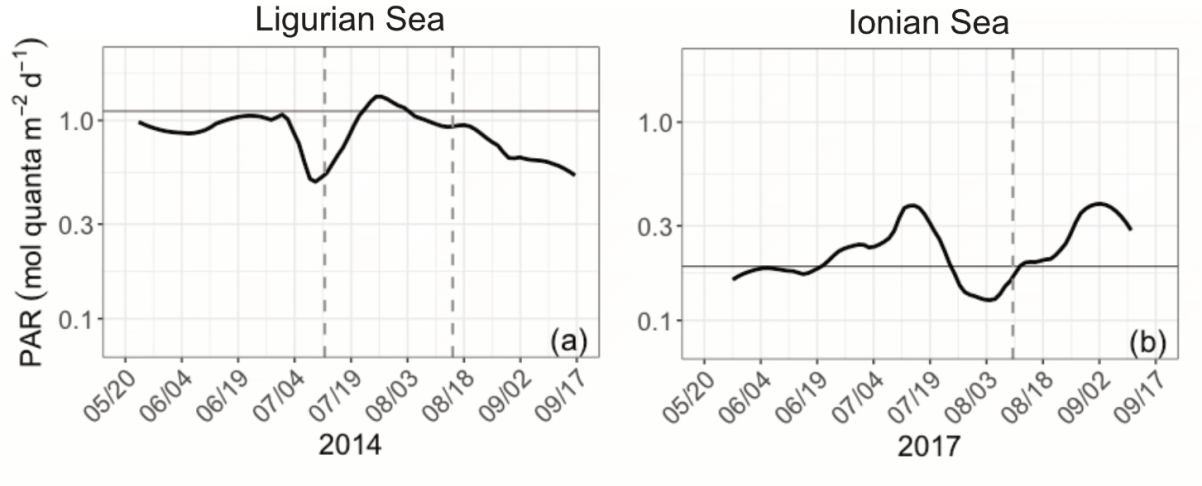

Figure 10: Time series of the daily-integrated photosynthetically available radiation (PAR) at the SCM level in the Ligurian Sea (a) and the Ionian Sea (b). The horizontal grey line shows the median of each time series. The dotted lines indicate the dates at which the values of c_p in the SCM layer reach a minimum.

APPENDIX A

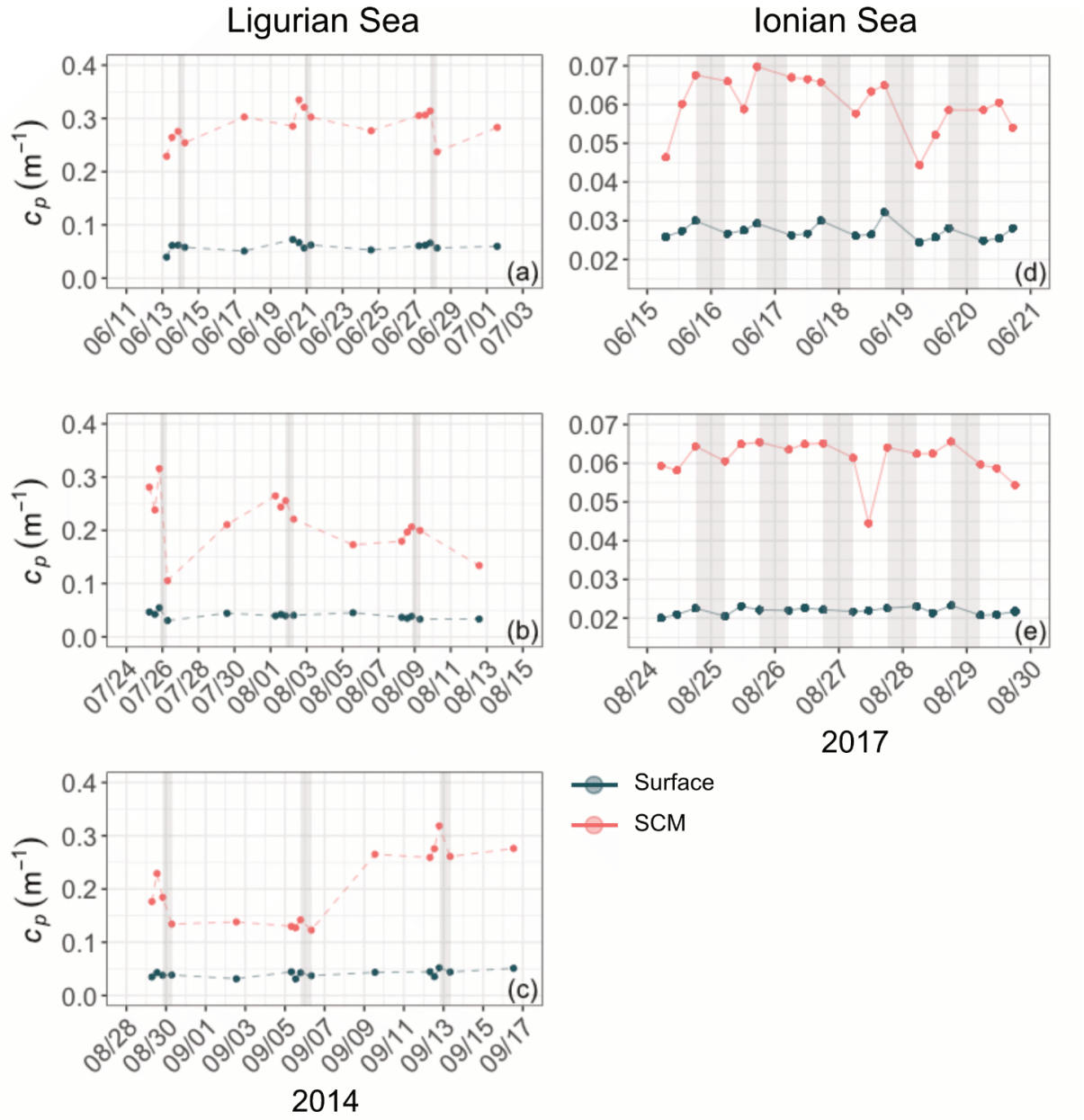

Figure A1: Example of time series of the c_p coefficient in the surface (red) and SCM (dark green) layers, chosen within the time periods indicated by the dashed lines in Figs 3-4, from May 24 to July 14, 2014 (a), July 14 to August 16, 2014 (b), and August 16 to September 13, 2014 for the Ligurian Sea (left), and from May 28 to August 11, 2017 (d) and August 11 to September 11, 2017 (e) for the Ionian Sea (right).

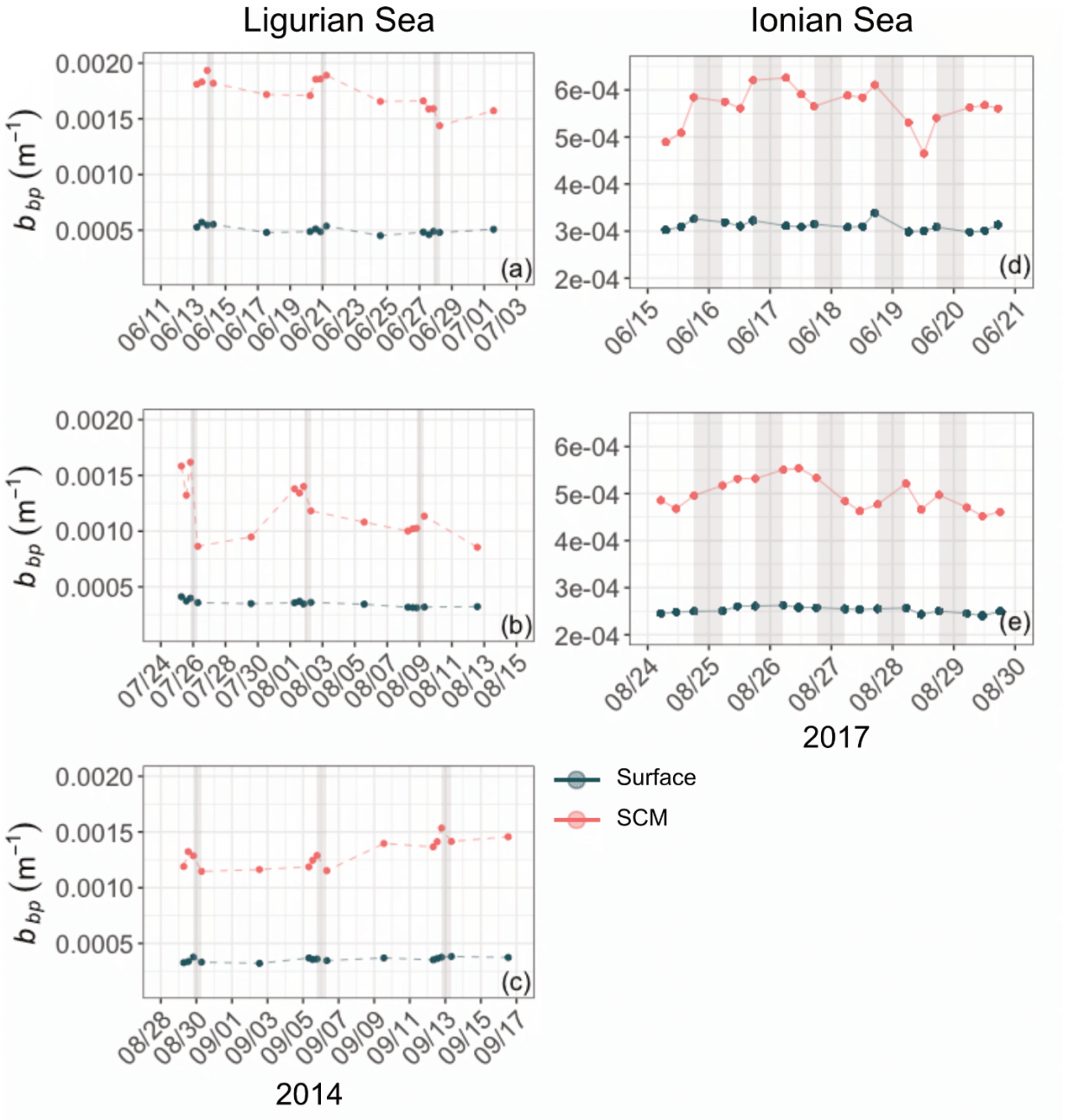

Figure A2: Example of time series of the b_{bp} coefficient in the surface (red) and SCM (dark green) layers, chosen within the time periods indicated by the dashed lines in Figs 3-4, from May 24 to July 14, 2014 (a), July 14 to August 16, 2014 (b), and August 16 to September 13, 2014 for the Ligurian Sea (left), and from May 28 to August 11, 2017 (d) and August 11 to September 11, 2017 (e) for the Ionian Sea (right).

APPENDIX B

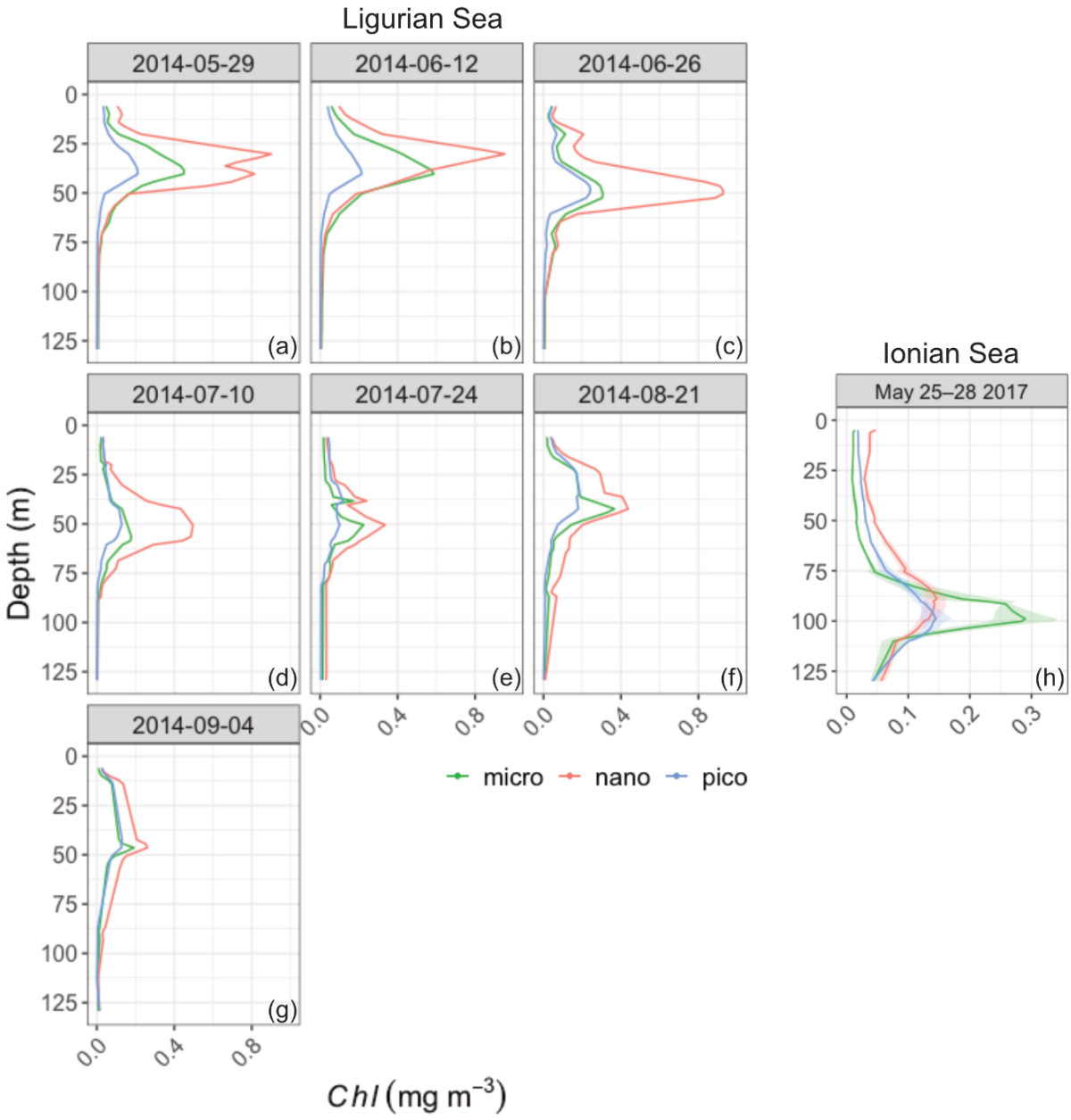

Figure B1: Vertical distribution of the chlorophyll *a* concentration of the micro- (green), nano- (red) and picophytoplankton (blue) derived from HPLC pigment determinations in the Ligurian Sea (BOUSSOLE site; a–h) and the Ionian Sea (PEACETIME cruise; i). For the Ionian Sea the solid line shows the mean value and the shaded area the standard deviation, calculated over a 4-day window (May 25–28, 2017).